



Appl. No. : 10/743,195
Applicant : Forrest Frank HOPKINS, et al.
Filed : April 6, 2004
Title : SYSTEM AND METHOD FOR DETECTING
AN OBJECT
Art Unit : 2882
Examiner : Krystyna Suchecki
Confirmation No. : 6880

Commissioner for Patents
P.O. Box 1450
Alexandria, VA 22313-1450

AFFIDAVIT UNDER 37 C.F.R. §1.131

Applicant provides this Affidavit in response to the Office action dated November 15, 2005 in the above-identified patent application. By this Affidavit, the assignee of the above-identified patent application (hereinafter the "Assignee") provides evidence to establish invention of the subject matter of the rejected claims prior to the effective date of the reference on which the rejection is based. Specifically, the assignee provides evidence of conception of the invention prior to the effective date of one of the cited references (Zhou et al.) coupled with evidence of due diligence from prior to that effective date to a subsequent reduction to practice or filing date of the above-identified patent application. The Assignee submits the following evidence:

1. Claims 1, 5-21, 25-48, 51-58 and 61-72 currently stand rejected under 35 U.S.C. § 103 as unpatentable over Krug in view of Zhou et al. Further, claims 3, 4, 23, 24, 49, 50, 59 and 60 currently stand rejected under 35 U.S.C. § 103 as unpatentable over Krug in view of Zhou et al. and Annis. Claims 1, 21, 41, 48, 58 and 68 are independent claims.
2. U.S. Patent Application Publication No. US 2004/0213378 to Zhou et al. has an effective date as a §102(e) reference no earlier than April 24, 2003, its effective filing date.

Best Available Copy

3. Claim 1 recites:

A system for detecting an explosive within an article, comprising:

an acquisition subsystem including an x-ray computed tomography scanner having a stationary radiation source and a stationary detector, said acquisition subsystem is adapted to acquire intensity measurements pertaining to the explosive; and

a reconstruction subsystem, in communication with the acquisition subsystem, for generating view data from the intensity measurements and for reconstructing the view data into image data representative of the explosive, wherein said reconstruction subsystem utilizes three-dimensional reconstruction techniques.

4. Appendix 1 includes a power point presentation, dated March 31, 2003, in which the claimed invention, including each of its elements, is discussed. Specifically, with reference to at least slide 3 of the power point presentation, there is mention of "Low-dose sCT", which is nomenclature for a stationary CT system that includes a stationary radiation source as well as a stationary detector. On that same slide is the mention of several "critical to quality" characteristics of such a CT system, including the ability to scan luggage, which is a multi-generational product development (MGPD) of Assignee. Further, on at least slide 7, there is discussion of an explosive detection system for possible development by Assignee for the Transportation Security Administration.

5. The power point presentation in Appendix 1 also includes a discussion beginning at slide 30 of reconstruction techniques under development. Specifically, in slide 33, there is mention of adaptive filtering reconstruction, which is done in three-dimensions.

6. Appendix 1 further includes several slides indicating the work to be done to reduce to practice the invention recited in claim 1. Specifically, at least slides 4, 8, 9, 13, 29 and 40 provide an overview of tasks to be performed to reduce to practice the invention recited in claim 1.

7. Assignee possesses additional evidence to support its conception of the invention recited in claim 1 prior to April 24, 2003 and due diligence until at least the filing of the above-identified patent application upon request of the Examiner.

8. Claim 21 recites:

A system for detecting an explosive within an article, comprising:

a transportation means for transporting the article;

an acquisition subsystem comprising an x-ray computed tomography scanning device having a stationary radiation source and a stationary detector and being adapted to acquire intensity measurements that can be generated into view data pertaining to the explosive;

a reconstruction subsystem, comprising a plurality of reconstruction stages, for reconstructing the view data into image data representative of the explosive, wherein said reconstruction subsystem utilizes three-dimensional reconstruction techniques; and

a computer-aided detection subsystem, comprising a plurality of computer-aided detection stages, for analyzing the image data.

9. At least slide 2 in Appendix 1 illustrates a transportation means for transporting an article. Further, the evidence on conception and reduction to practice posed above regarding claim 1 is equally applicable to claim 21 as it applies to the acquisition subsystem and the reconstruction subsystem.

10. Appendix 2 includes an email sent March 26, 2002 from Ricardo Avila, one of the inventors of the above-identified patent application. The email message indicates that the attachment to the email (also in Appendix 2) is a long term explosive detection system proposal including the computer-aided detection subsystem element. Please note that Figure 1 of the proposal is very similar to Figure 1 of the above-identified patent application. Further, Figure 7 of the attachment shows a stack of CT slices that have been processed with volume rendering techniques to create a three-dimensional image of the interior of a piece of luggage.

11. Appendix 3 includes a screen shot of the source code repository at Assignee's

Global Research Center in Niskayuna, New York. The screen shot indicates that the source code “vtkImageHessianResponse.cxx”, which implements a Hessian filter, was downloaded into the system at least as early as December 27, 2002. This evidence indicates that the inventors of the above-identified patent application had in their possession a computer-aided detection subsystem for analyzing image data, as recited in claim 21, prior to April 24, 2003.

12. Appendix 4 includes an e-mail, dated January 23, 2003, to Ricardo Avila, one of the inventors of the above-identified patent application, and referring to a Final Report sent to L-3, then a customer of Assignee. The e-mail states “The Vector Hessian (VHess) algorithm has detection rates that are comparable to but slightly lower than the EDS version 104 software”. The significance of this e-mail and this statement is that they evidence that the inventors had incorporated the computer-aided detection subsystem with an acquisition subsystem and a reconstruction subsystem prior to April 24, 2003.

13. Assignee possesses additional evidence to support its conception of the invention recited in claim 21 prior to April 24, 2003 and due diligence until at least the filing of the above-identified patent application upon request of the Examiner.

14. Claim 41 recites:

A system for detecting an explosive within an article, comprising:

an acquisition subsystem including an x-ray computed tomography scanner for acquiring intensity measurements pertaining to the explosive;

a reconstruction subsystem, in communication with the acquisition subsystem, for generating view data from the intensity measurements and for reconstructing the view data into image data, wherein said reconstruction subsystem utilizes three-dimensional reconstruction techniques;

a computer-aided detection subsystem for analyzing the image data; and

at least one additional source of information pertaining to the explosive, wherein the image data and the at least one additional source of information assist in identifying the explosive.

15. The evidence on conception and reduction to practice posed above regarding claim 1 is equally applicable to claim 41 as it applies to the acquisition subsystem and the reconstruction subsystem. Further, the evidence on conception and reduction to practice posed above regarding claim 21 is equally applicable to claim 41 as it applies to the computer-aided detection subsystem.

16. Further, Appendix 1 includes, in at least slide 3, a discussion of energy-discrimination computed tomography (EDCT), which is included as an additional source of information as recited in claim 41. Furthermore, in at least slide 29, the task of EDCT benefiting sCT is mentioned as a deliverable in the third quarter of 2003, thus evidencing due diligence to reducing EDCT in sCT to practice.

17. Assignee possesses additional evidence to support its conception of the invention recited in claim 41 prior to April 24, 2003 and due diligence until at least the filing of the above-identified patent application upon request of the Examiner.

15. Claim 48 recites:

A method for detecting an explosive within an article, comprising:

acquiring information pertaining to the explosive with an acquisition apparatus having an x-ray computed tomography scanner with a stationary radiation source and a stationary detector; and

reconstructing an image representative of the explosive based upon the acquired information, wherein said reconstructing includes reconstructing the acquired information into a three-dimensional image.

18. The evidence on conception and reduction to practice posed above regarding claim 1 is equally applicable to claim 48 as it applies to the acquiring information with an x-ray computed tomography scanner having a stationary radiation source and stationary detector and reconstructing a three-dimensional image.

19. Assignee possesses additional evidence to support its conception of the

invention recited in claim 48 prior to April 24, 2003 and due diligence until at least the filing of the above-identified patent application upon request of the Examiner.

20. Claim 58 recites:

A method for detecting an explosive within an article, comprising:

acquiring information pertaining to an object located within the article with an x-ray computed tomography machine having a stationary radiation source and a stationary detector;

communicating the acquired information to a plurality of reconstruction modules;

reconstructing the acquired information into image data with the plurality of reconstruction modules, wherein said reconstructing includes reconstructing the acquired information into a three-dimensional image; and

analyzing the image data to identify whether the object is an explosive device.

21. The evidence on conception and reduction to practice posed above regarding claim 1 is equally applicable to claim 58 as it applies to the acquiring information with an x-ray computed tomography scanner having a stationary radiation source and stationary detector and reconstructing a three-dimensional image.

22. Further, the information provided in Appendix 4 is significant in that it evidences that the inventors had incorporated the computer-aided detection subsystem with an acquisition subsystem and a reconstruction subsystem prior to April 24, 2003, thereby communicating the acquired information and analyzing the image data as recited in claim 58.

23. Assignee possesses additional evidence to support its conception of the invention recited in claim 58 prior to April 24, 2003 and due diligence until at least the filing of the above-identified patent application upon request of the Examiner.

24. Claim 68 recites:

A method for detecting an object, comprising:

scanning an article with an x-ray computed tomography machine to acquire information pertaining to the object, wherein the computed tomography machine includes a stationary radiation source and a stationary detector;

discriminating between high-energy and low-energy signatures;

reconstructing image data representative of the object based upon the high-energy and low-energy signatures, wherein said reconstructing includes reconstructing the information derived from the high-energy and low-energy signatures into a three-dimensional image; and

analyzing the reconstructed image to identify the object.

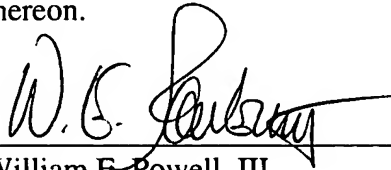
25. The evidence on conception and reduction to practice posed above regarding claim 1 is equally applicable to claim 68 as it applies to scanning an article with an x-ray computed tomography scanner having a stationary radiation source and stationary detector and reconstructing a three-dimensional image. Further, the evidence on conception and reduction to practice posed above regarding claim 41 is equally applicable to claim 68 as it applies to discriminating between high and low energy signatures and as it applies to reconstructing information derived from high and low energy signatures.

26. Assignee possesses additional evidence to support its conception of the invention recited in claim 68 prior to April 24, 2003 and due diligence until at least the filing of the above-identified patent application upon request of the Examiner.

27. Assignee submits that, in accordance with the above remarks and the accompanying Appendices, it has established conception of the invention of the subject matter of the rejected claims prior to April 24, 2003 and, at the very least, due diligence until constructive reduction to practice, namely the filing of the above-identified patent application.

28. All statements made by the declarant herein that are based on personal knowledge are true and all statements based on information and belief are believed to be true. These statements are made with the knowledge that willful false statements and the like so made are punishable by fine or imprisonment or both, under section

1001 of Title 18 of the United States Code, and that such willful false statements may jeopardize the validity and/or enforceability of the application or any patent issuing thereon.

A handwritten signature in black ink, appearing to read "W.E. Powell, III", is written over a horizontal line.

William E. Powell, III

Patent No. 39,803

Supervisory Patent Attorney

General Electric Company

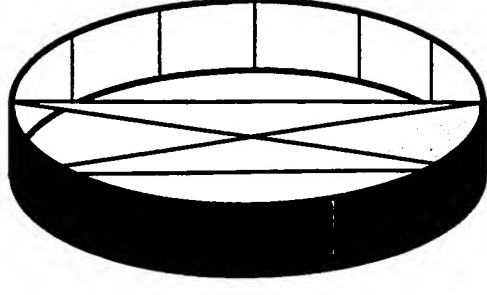
Appl. No. 10/743,195

139681-2

Reply to Office action of November 15, 2005

Appendix 1

- Future CT applications demand volume coverage at low dose
 - Cardiac imaging
 - Perfusion
 - Screening applications
- Present CT systems have fundamental limitations
 - 3rd generation: Scan speed; coverage
 - EBCT: Coverage; cost; geometry, limited scan range due to geometry
- Potential new opportunities
 - Organ in rotation
 - Functional Imaging
 - Industrial applications including EDS, GEIT



Low-Dose sCT is the vision for future CT technology

Low dose:

- ED for contrast
- New recon
- No septa

20 ms scan speed

Source:

- Field emitters
- Flexible geometry

160 mm coverage

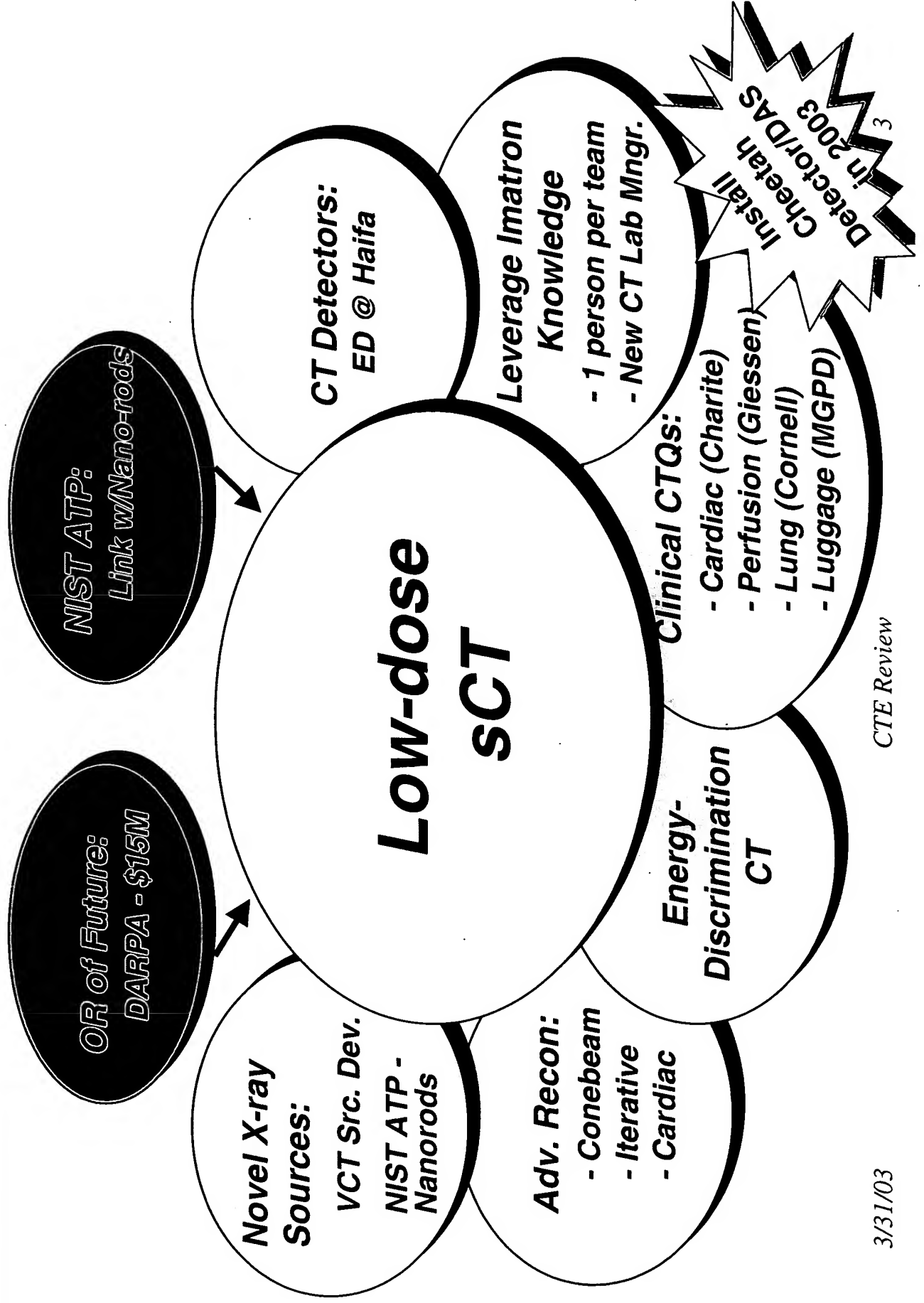
High speed Detector/DAS

Recon:

Eliminates noise penalty of FBP

Picovoxel

Low-Dose sCT: high resolution(30 lp/cm), large volume coverage(16 cm), fast scanning(20 ms), dose reduction



1. Demonstrate arc source feasibility & functionality
2. Commence nanotube development - complement NIST Nanorods
3. Quantify IQ of 5th Generation sCT technology
4. Develop methods(recon and preprocessing) for low-dose
5. Secure key IP for low-dose sCT technology

*Build upon 2001 and 2002 efforts to deliver on these
2003 objectives*

Field emitter based x-ray arc source

- Field emitter availability & robustness
- Flux output

Image Quality

- Low Contrast Detectability (LCD)
 - Flux Output
 - Scatter noise
- Aliasing artifacts, full-FOV resolution
- Cone-beam artifacts
- Low dose scanning

2003

Detector

- High speed scintillator – capitalize on LuTAG
- Energy discriminating detector

DAS speed

- ~20x greater than Lightspeed
- Noise

Cost

- X-ray source technology
- Volume detector ring (EDCT)
- DAS

2004

Focus on field emitter source & IQ early in plan –
prove-out of sCT technology

- **Transportation Security Administration - Security Initiatives**

- **Explosive Detection System (EDS)** – White December 2002
 - \$40M estimate (+\$9M for CAD)
 - Bill McGann (VP R&D, Ion Track) will visit TSA on Feb. 4th
 - baggage scanning (\$200k MGPD) and query about TSA BAA date.

Need commercial system in 3 years
 - will consider 3rd generation w/stationary anode

- **Defense Advanced Research Projects Agency (DARPA)**

- “OR of the future” - White paper submitted January 2003
 - \$15M estimate (no ED)

- **National Institute of Standards & Technology (NIST) – Advanced Technology Program (ATP)**

- Accelerates development of innovative technologies that offer widespread benefits to the nation
- Leverage ongoing Nano-rod 3-year \$5.8M program

- ✓ Demonstrate arc source feasibility & functionality
- ✓ Validate flux output capability of FE technology
- ✓ Commence Carbon Nano-tube program to complement NIST ATP
- ✓ Quantify baseline IQ attainable with sCT technology due to flux, scatter
- ✓ Quantify IQ benefits of low-dose recon methods: iterative recon & adaptive filtering
- ✓ Devise integrated technology roadmap for sCT
- ✓ Secure key IP for low-dose sCT technology
- ✓ Identify and target key funding sources to support low-dose sCT development

4Q03 – Know limits of IQ - provide vision to realize the goal: a “Revolution” in CT ... with no rotation

Risks

1. Field emitter current density too low
2. Mechanical and electrical design

2003 Abatement Plans

- ✓ Initiate in-house field emitter technology development
- ✓ Proof of concept: buy available devices from research community
 - ANI (Carbon Nanotubes) , SRI (Spindt)
- ✓ Demonstrate arc source feasibility & functionality - Validate flux output

*Develop arc source in-house – components and devices –
to maximize GE-owned IP*

What is an arc source?

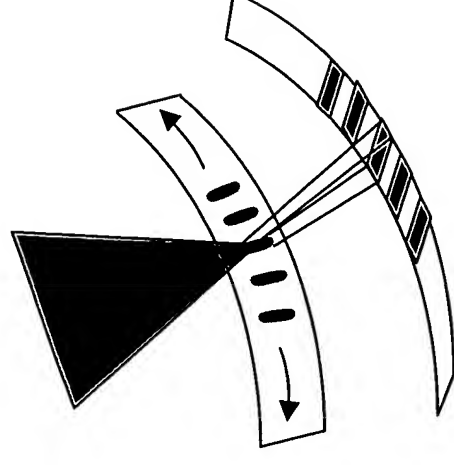
- A distributed x-ray source enabling sCT speed and compact geometry

Key technologies:

- Field emission electron sources
- Beam sweeping electron optics
- High frequency control electronics
- Integrally cooled focal track

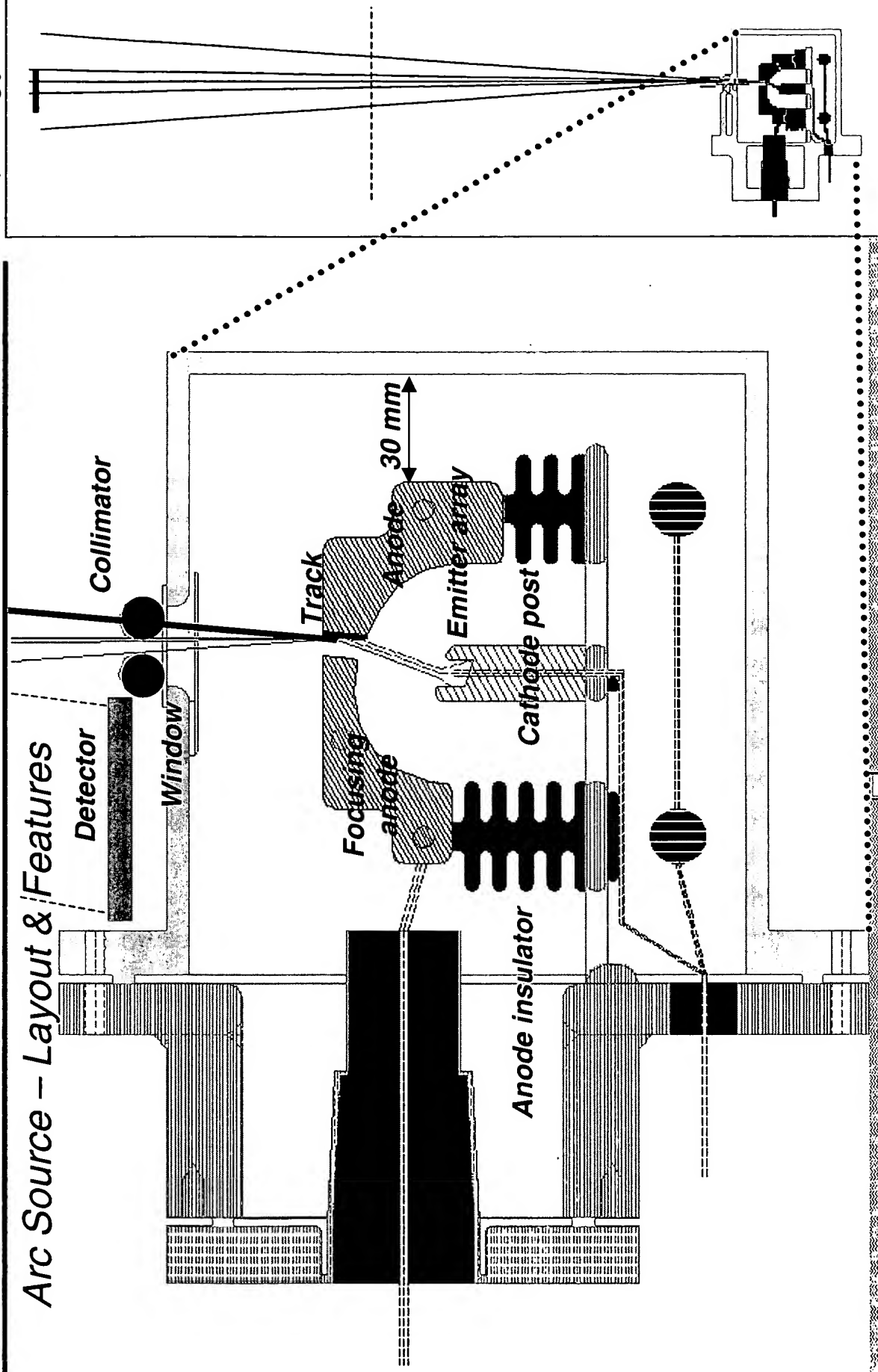
Deliverables ('03):

- Technology demonstrator partial arc source
- Multispot, fast rise and dwell times
- Continue to lock up critical IP on source design




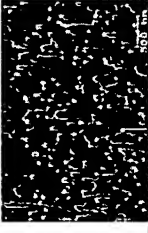

Key enabling technology for sCT

Arc Source – Layout & Features



Challenging technology – strong IP position

Eight "cold cathode" technologies investigated in '02, 3 downselected

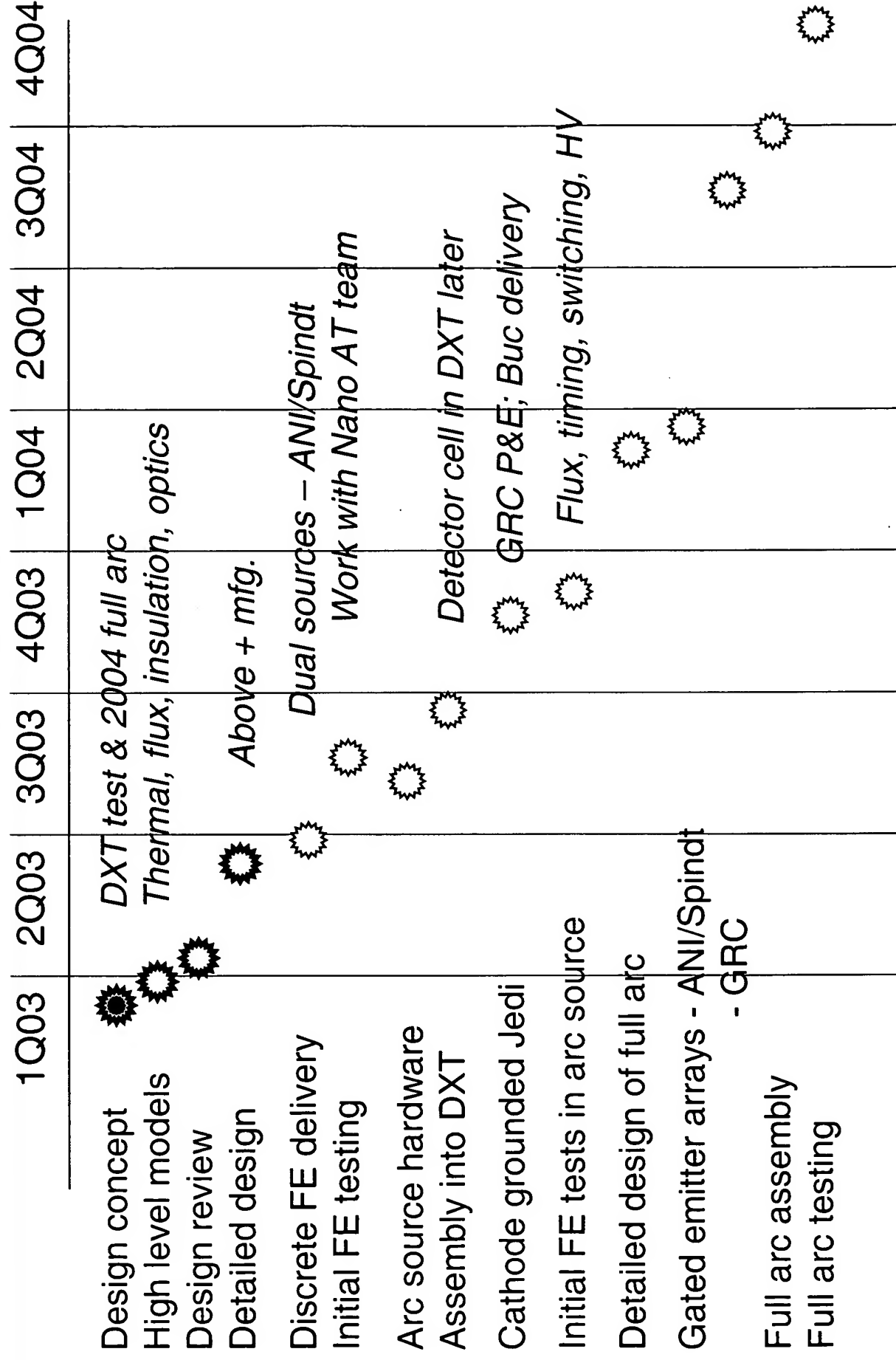
<i>Emitter Type</i>	<i>Technology status</i>	<i>Development status for sCT</i>	<i>GE IP potential</i>
Nanorods/wires 	Immature	\$3M / 3 yr. @GRC (NIST/AT)	Emitter materials, fabrication, device <i>Assessing landscape</i>
Carbon nanotubes 	Broad effort in research community <i>Limited research for x-ray -- not proven</i>	Initiated in-house development	Emitter materials, fabrication, devices <i>Licensing required</i>
Spindt tips 	20+ year history; devices available <i>Not robust: Need high vacuum, tip blunting</i>	Risk mitigation	Emitter materials, fabrication, devices

Critical technology:

- Short-term: Purchase available devices
- Mid-term: In-house Carbon Nanotubes
- Long-term: Nanorods

No development with suppliers

\$1.2M total in 2003
for arc-source development



Comprehensive risk analysis performed by source team



- 40 risks identified in 10 sub-areas
- Abatement plans in place for top 10 risks – others to be tracked

Top risk – field emitter technology development

- Dual source from research groups (ANI, SRI)
- Nanorod program in place at GRC with NIST & AT funding – long term plan
- Parallel effort initiated in 2003 on CNT's at GRC

Focusing on retiring top level risks in 2003

Anode: *Optimized x-ray output over FOV for $\sim 10 \mu s$ pulses*

- Monte Carlo tool for flux prediction (used for VCT also)
- System geometry tool for focal spot sizing
- Maximum mA predicted for various operational modes
- First order electron backscatter models complete
- Off-focal radiation modeling identified as critical need
- Novel focusing anode target geometry developed – IP

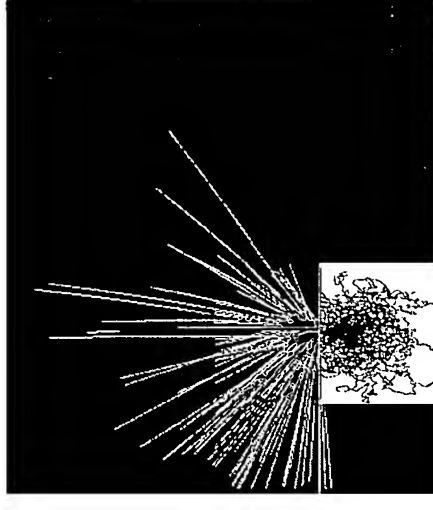
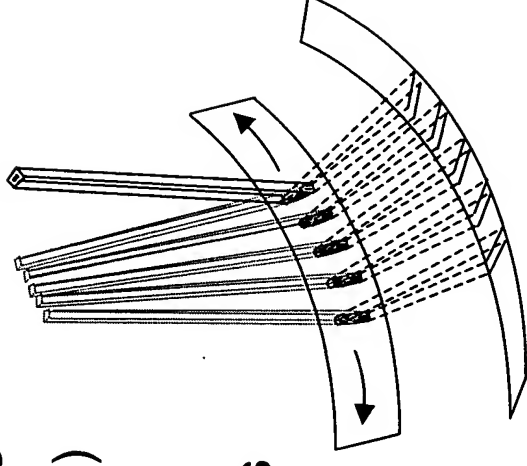
pending

Flux model

Geometry

Vacuum vessel: *Compact design for full arc*

- Demountable X-ray tube testing in 2003
- Electron backscatter and off-focal radiation modeling



Building on Imatron technology

Electron Optics: *Validated electron beam profiles*

- Goal is 0.6 isotropic spot
- 2D Modeling – width meets spec; length next
- 3D modeling next



Controls: *<1 μ s rise times for available FEs*

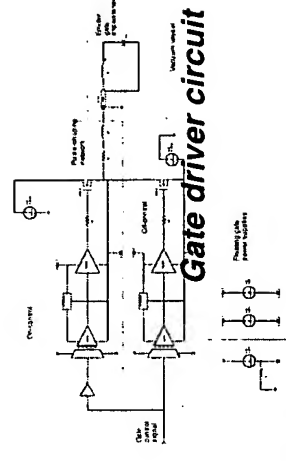
- System architecture draft complete
- Gate circuit designed
- Vacuum integration underway

Generator: *Cathode ground Jedi (1150 mA/160 kV)*

- Order in-place w/Buc FW 13 (P&E funded)
- Delivery expected early November

The key sCT differentiator

System architecture



[illegible]

$$\varepsilon = \text{asin}\{[\text{SID} + \text{sqrt}(\text{IDD}^2 - (\text{FOV}/2)^2)] \sin \delta / \text{IDD}\}$$

3/31/03

Low Dose Stationary CT

SCT x-ray & electron beam design

independent			system geometry	
focal spot length on target	L	mm	focal spot sizes	
focal spot width on target	w	mm		
target angle	α	deg		
detector z-offset	z_d	mm	x-ray flux	
source-iso distance	SID	mm	emitter specifications	
iso-detector distance		mm		
dependent				
detector width in z	w_d	mm	295	
minimum detector z-offset to clear source cone	z_{dmin}	mm	26.1	
near cone angle	γ_1	deg	0.5	
far cone angle	γ_2	deg	11.8	
source fan half angle	δ	deg	18.2	
detector fan half angle	ϵ	deg	41.4	
minimum focal spot length on central plane at isocenter	l_{min}	mm	0.60	
focal spot length at target side of detector projected to isocenter	l_1	mm	0.71	
focal spot length at far side of detector projected to isocenter	l_2	mm		
focal spot width at center of fan	w	mm	0.6	
f.s. width at end of fan seen \perp to beamline	w_δ	mm	4.81	
f.s. width at end of fan seen \perp to detector surf.	w_ϵ	mm		
electron beam current	mA	mA	3.3	
electron beam length \perp to e-beamline	L_b	mm	4.7	
emitter length	L_e	mm	14.0	
Beam on time (swept focal spot)	t_{swept}	μs	2.4	
Beam on time (fixed focal spot)	t_{fs}	μs	10	
% of track used for focal spots (fixed focal spot)	-	-	0.24	
beam sweep required for continuous beam		mm	0.46	
current density in e-beam	j_b	A/cm ²	26.3	
current density at emitter surface	j_e	A/cm ²		
x-ray photon flux at end of detector closest to target	ϕ_1	ph/s/cm ²		
x-ray photon flux at far end of detector (heel effect)	ϕ_2	ph/s/cm ²		
x-ray intensity measured at detector 1450 mm away (zero plane)		ph/s/cm ²		



Low Dose Stationary CT

FS degradation
within FOV:
2.5x

SCT system parameters:

SID 800; IDD 675

System CTQs	# views	focal spot spacing in theta mm	scan time s	view time μ s	scan arc length deg	system		target angle deg	f.s. length mm	beam res. μ s	mA	mA-s per scan
						f.s. length mm	f.s. width mm					
Source CTQs	-	-	-	-	-	-	-	-	-	-	-	-
	704	-	0.4	568	-	1.2	1.2	7	9.8	14.1	800	320
	704	-	0.5	710	360	0.7	0.9	7	5.7	10.5	300	150
eSpeed	2602	-	0.05	19.2	210	2.6	1.1	12.5	12.0	16.7	1000	50
SCT (fixed beams)	1167	2.5	0.02	17.1	210	0.6	0.6	7	5.8	17.1	733	15
	2000	2.5	0.02	10	360	0.6	0.6	7	5.8	10.0	970	19
	2000	1.5	0.02	10	210	0.6	0.6	7	5.8	10.0	966	19
SCT (swept beam)	2000	2.5	0.02	10	360	0.6	0.6	3	13.6	10.0	2221	44
	1167	2.5	0.02	17.1	210	1	1	3	22.6	17.1	4393	88
	1167	2.5	0.02	17.1	210	0.6	0.6	3	13.6	4.1	3353	67
	1167	1.5	0.02	17.1	210	1	1	3	22.6	6.8	6483	130

Some concepts in the range of
Lightspeed and Imatron

FS degradation
within FOV:
4.2x



Low Dose Stationary CT

Risk Areas	Date
Window	1-Jan-03
Cooling	1-Jan-03
High voltage	1-Jan-03
HV Insulator	1-Jan-03
Interface electronics	1-Jan-03
Field emitters	1-Jan-03
Drive electronics	1-Jan-03
Emitter packaging	1-Jan-03
Vacuum chamber	1-Jan-03
Target	1-Jan-03

Target

SCORE
ACTUAL
PLAN

Emitter packaging

SCORE
ACTUAL
PLAN

Drive electronics

SCORE	SCORE
ACTUAL	red
PLAN	yellow
1 Target detachment from cooling window	green
Initial simulation shows a peak in thermal loading for an instantaneous window for 120kV x 350mA instantaneous FS) - this is about 5 times higher than the electron collector and Be window temperatures within Limits?	SCORE
2 temperatures within Limits?	red
Peak Thermal loading on the window for 120kV x 350mA instantaneous input power is deposited on the window on the Track?	yellow
3 on the Track?	green
Backscattered electrons from the region in front (opposite) of the target assembly is localized in high intensity loading (45 MW/sq-m for 120kV x 350mA instantaneous loading) which may cause meltdowns in copper.	SCORE
4	red
1 Emitter gate voltage specs. In flux	yellow
2 Emitter current may be very sensitive to gate voltage	green
3 High gate voltages (up to 2kV)	
4 Emitter pulse width specs. Not defined	
5 Gate drive does not survive spits	

4



Risks – IQ Capabilities of sCT

1. Reduced Low Contrast Detectability(LCD)
2. Aliasing artifacts, full-FOV resolution
3. Cone-beam artifacts

2003 Abatement Plans

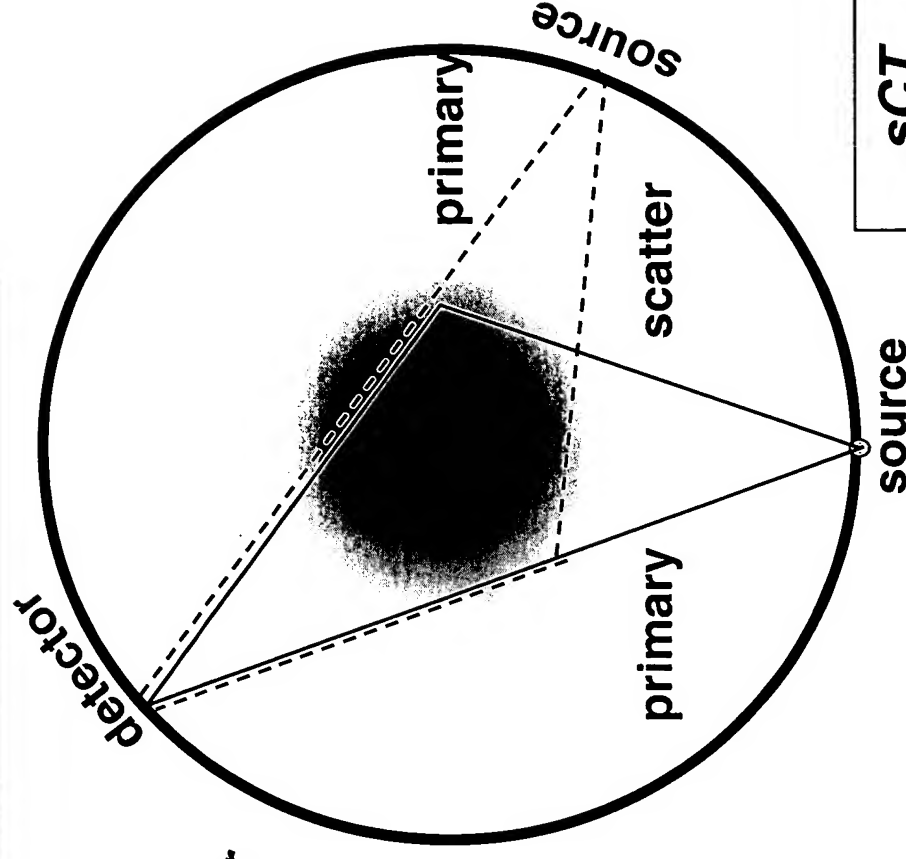
- ✓ Simulate/validate scatter signals – large coverage
- ✓ Quantify LCD: tube output, DAS noise, scatter noise
- ✓ Quantify benefits of novel low-dose recon strategies
 - Iterative Recon & Adaptive filtering
- ✓ Execute simulations to estimate view rate

*Leverage company-wide efforts:
GEGR, MKE, Hino, external collaborations*



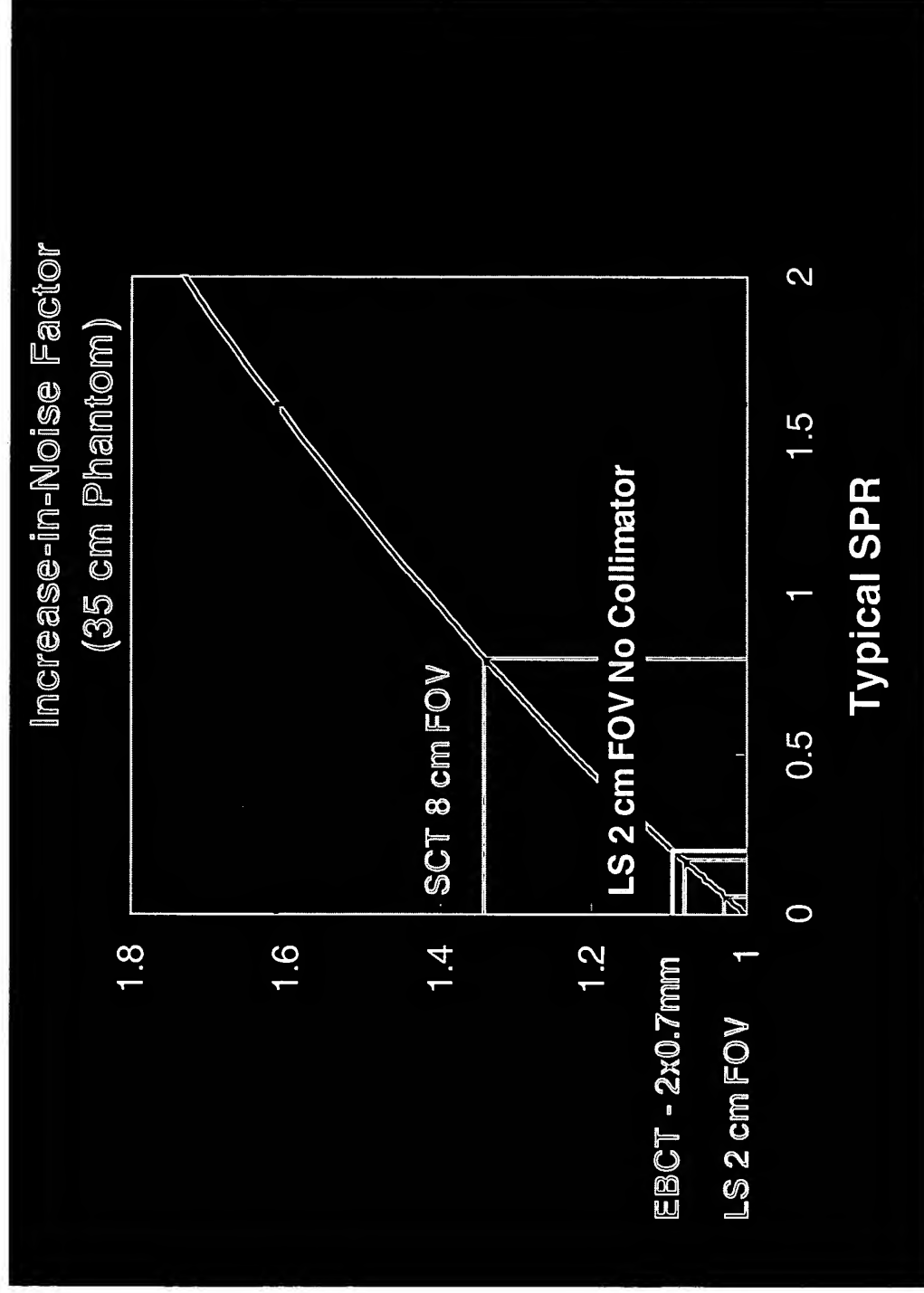
Lightspeed

- 3rd Generation CT: detector - source configuration fixed
- Collimators used to reject scatter



sCT

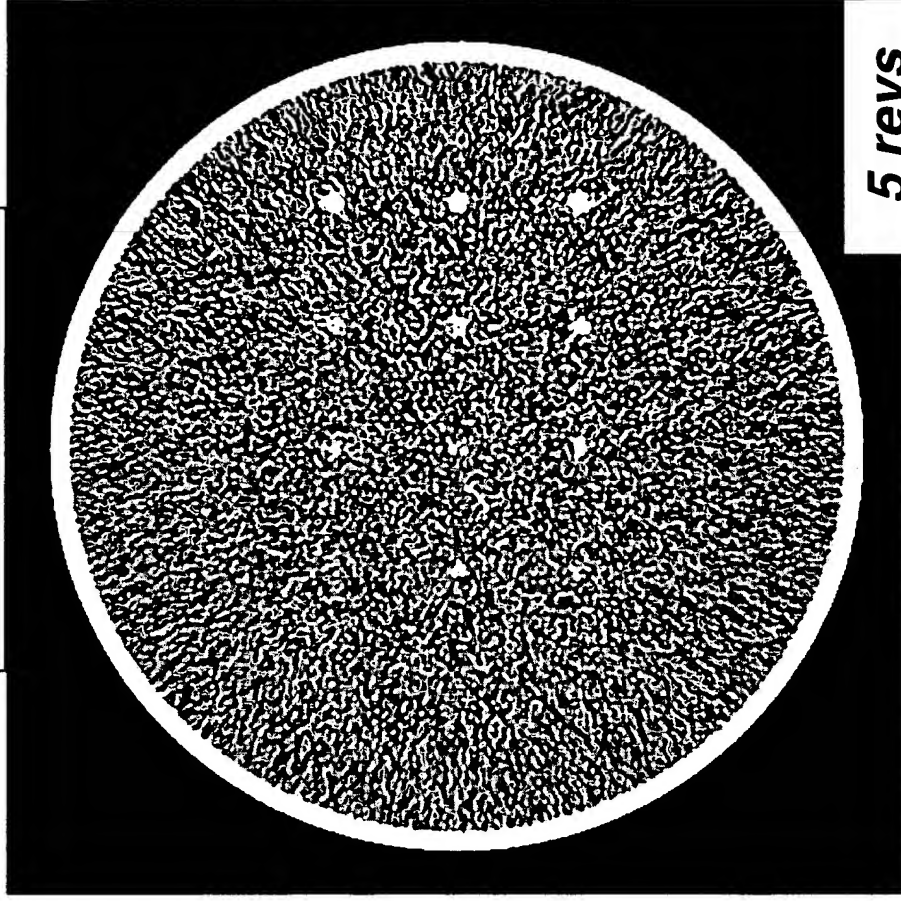
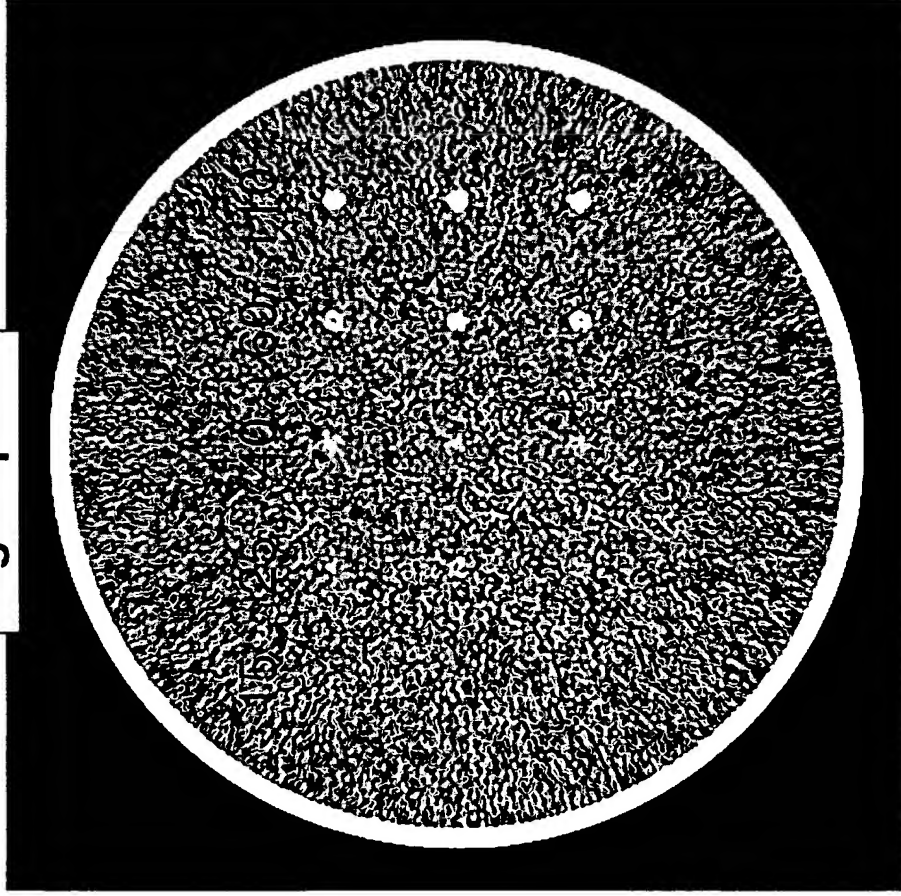
- 5th Generation CT: detector - source configuration not fixed
- Collimation not viable



sCT geometry: large increase of scatter in measurements – negatively impacts IQ

LightSpeed

sCT - no scatter



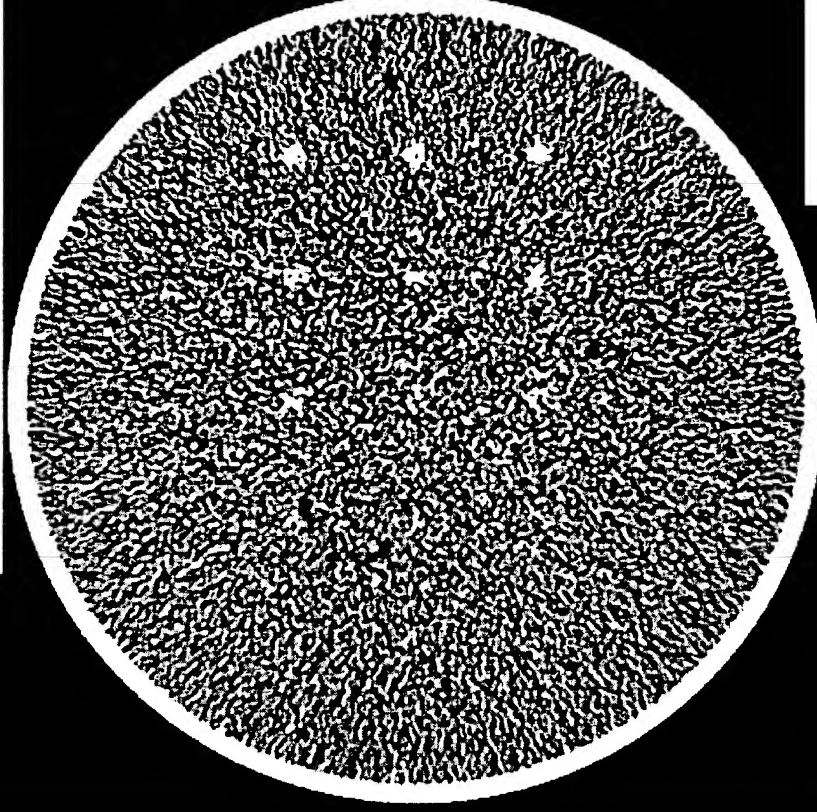
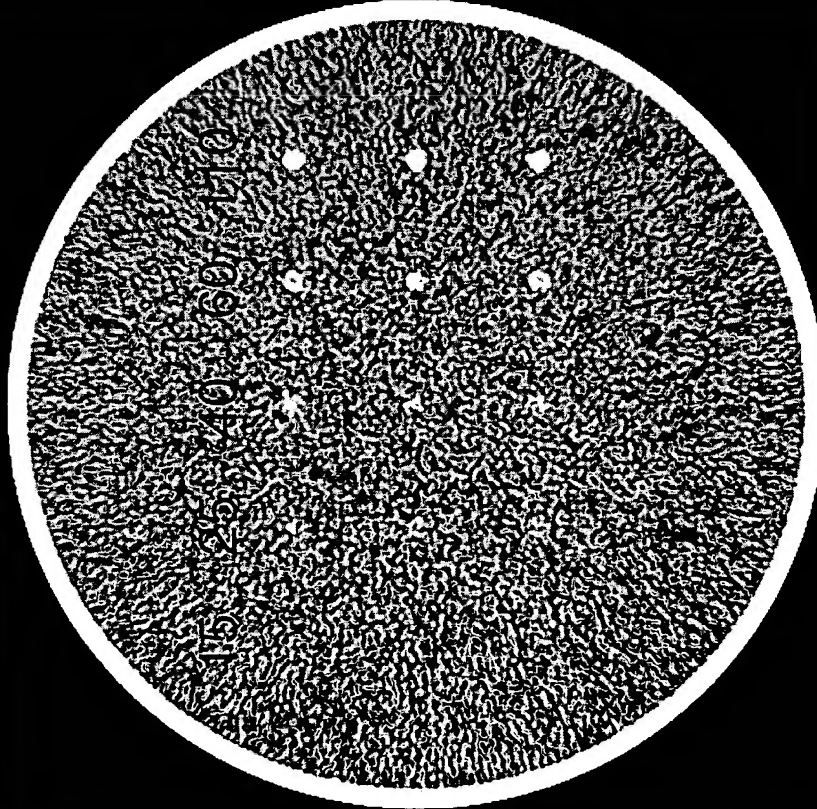
5 revs

100mAs, 20cm water Level=0, Window=100

System Geometry has slight impact on LCD

LightSpeed

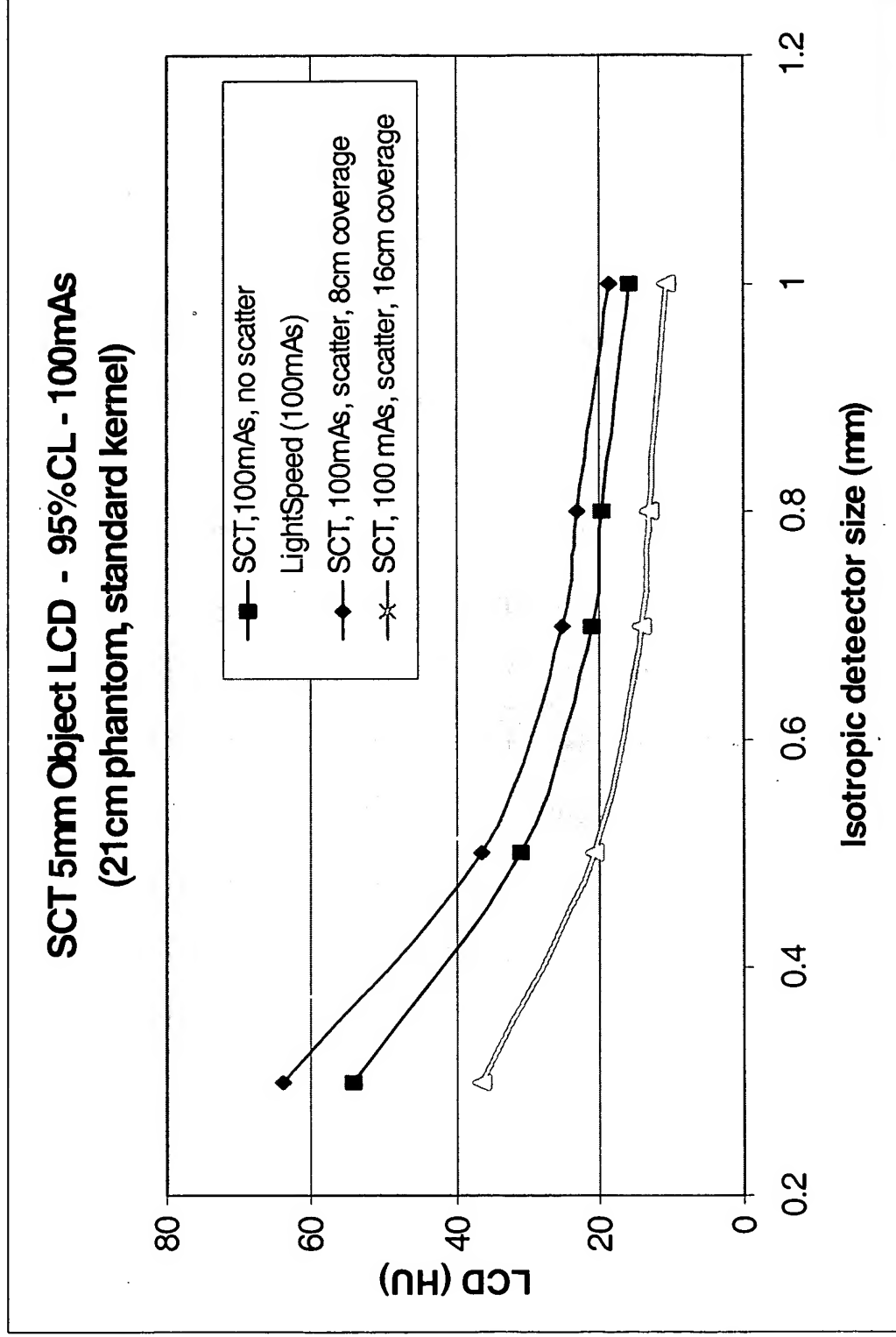
sCT – inc. scatter
(SPR=80%)



5 revs

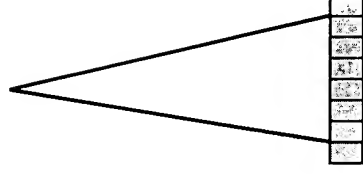
100 mAs, 20 cm water Level=0, Window=100

Residual Scatter Noise – Significantly reduces LCD

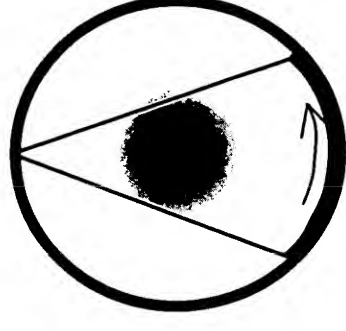


$LCD \propto 1.0/\text{pixsize}$

- Optimize design with respect to scatter
- Investigate approaches for scatter correction
 - Novel collimators
 - Measure scatter with detector elements that are outside field of view
 - Dual energy scatter subtraction

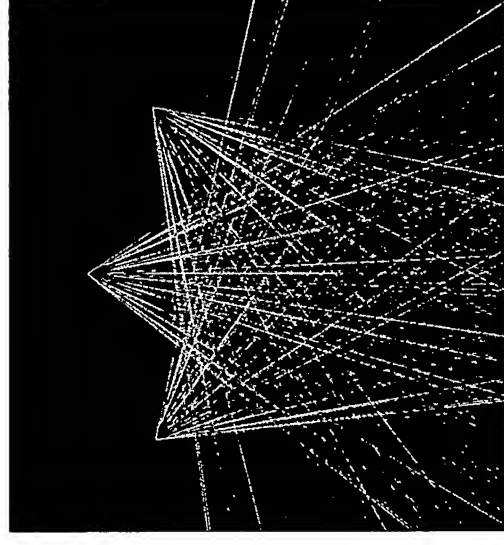
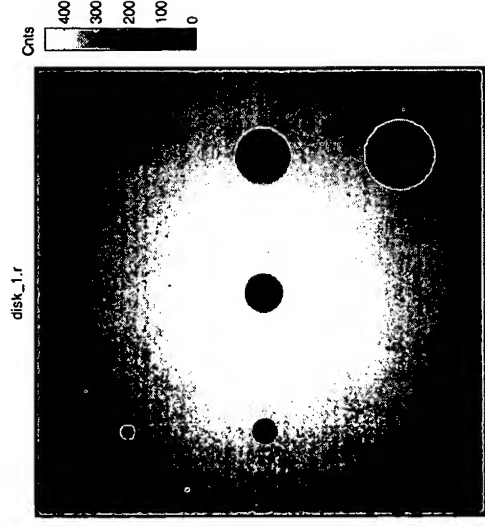


Scatter-dedicated detector elements

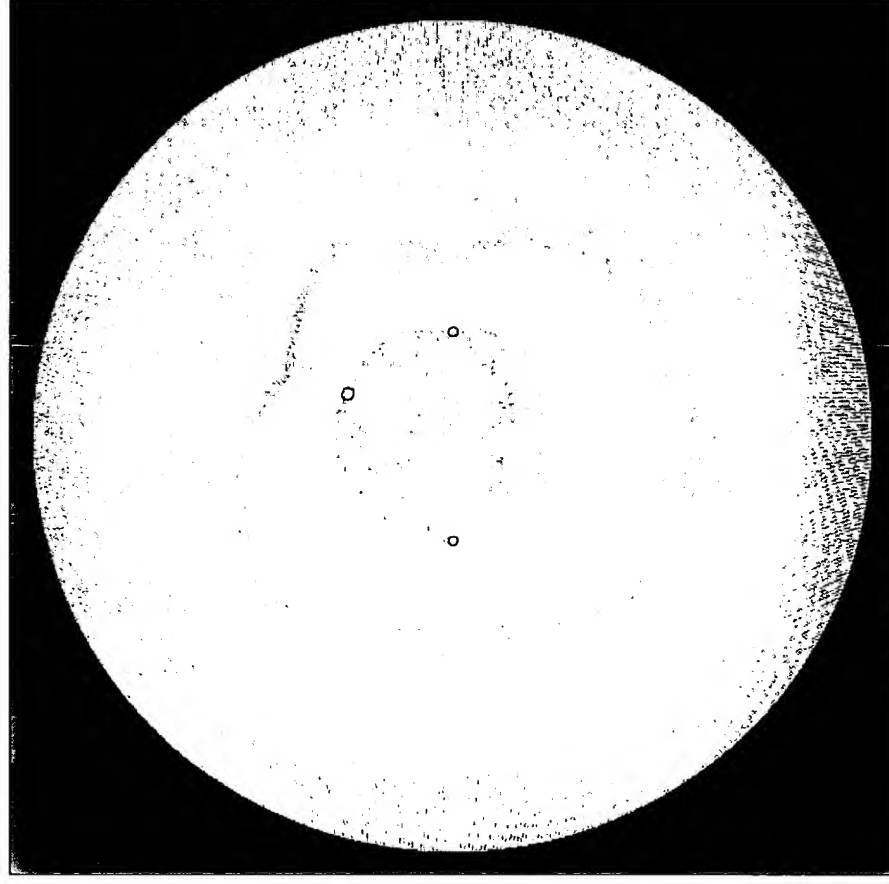


Rotating collimator

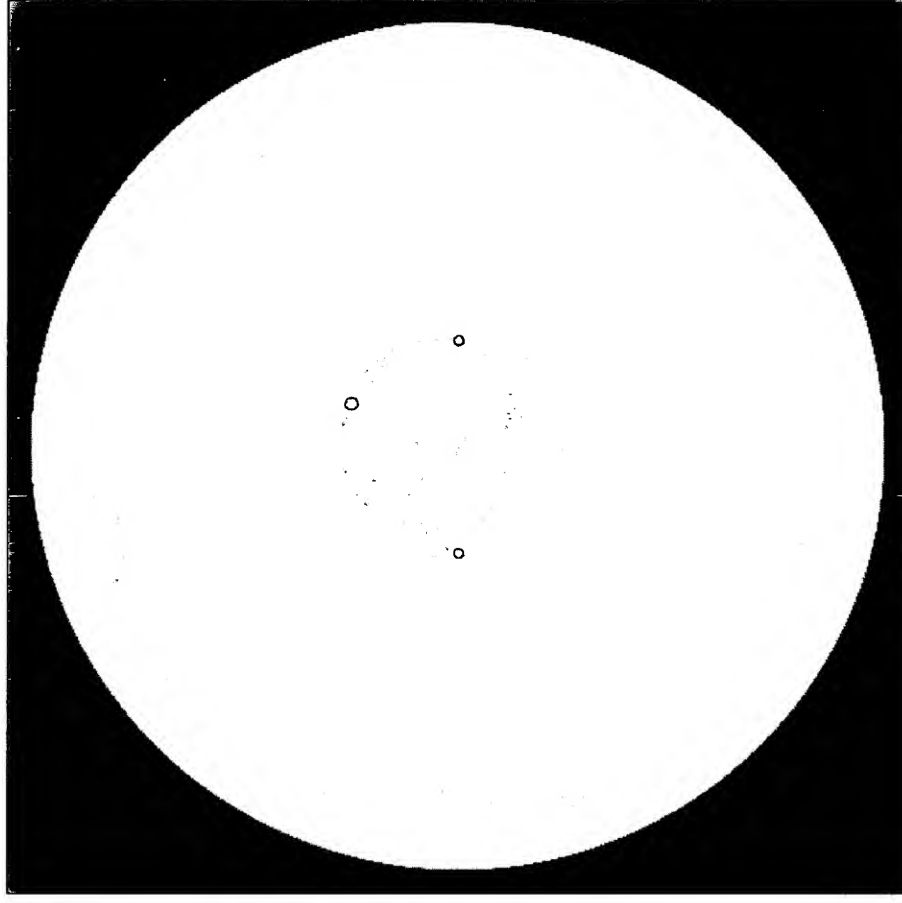
Use simulation (VRAI) for optimization of system and reconstruction
 Make experimental measurements where practical and to validate simulation



1000 views



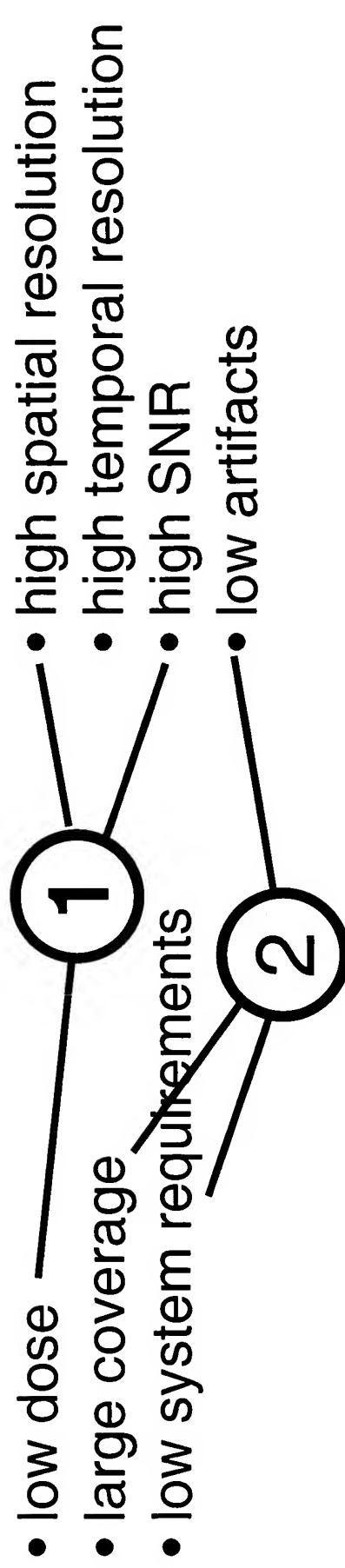
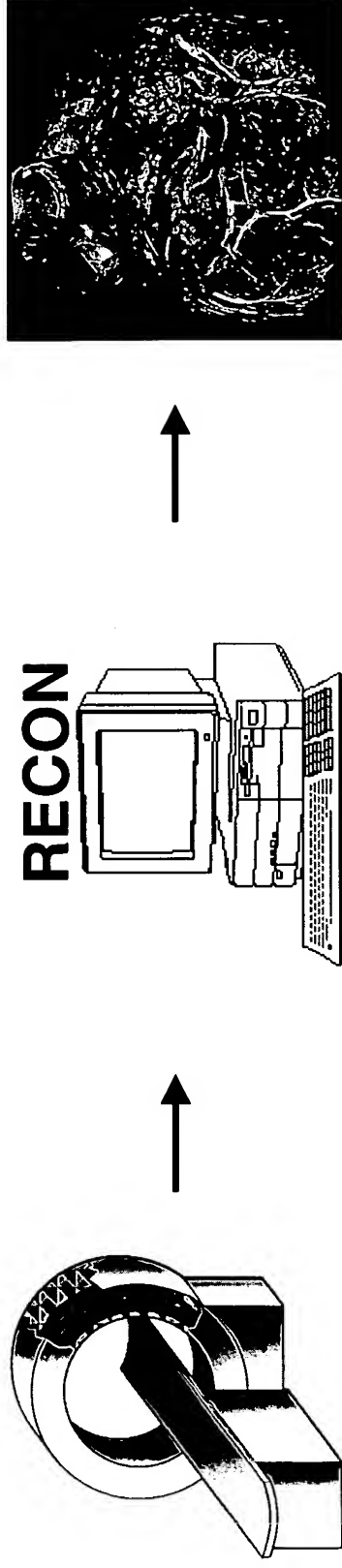
2000 views



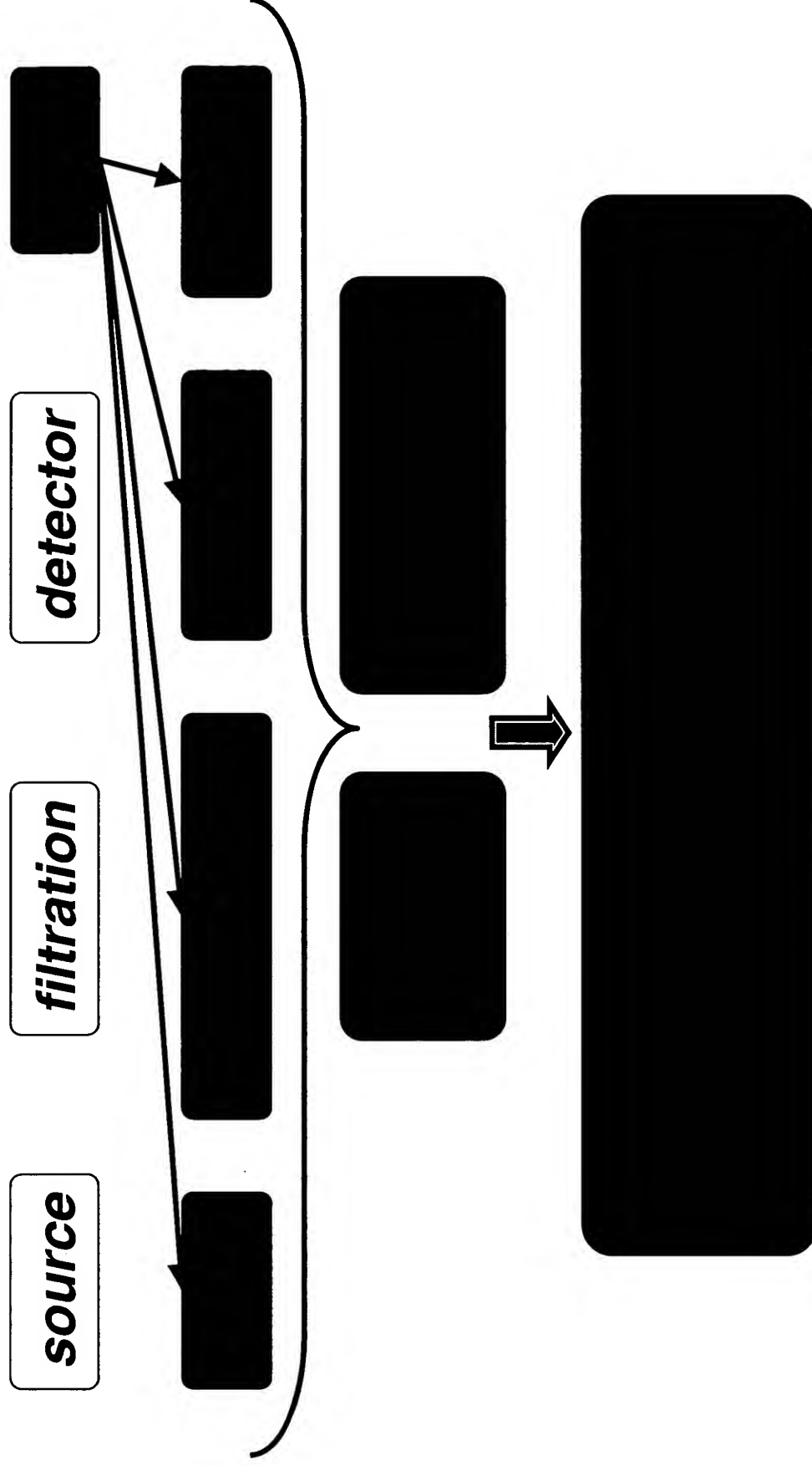
Executing simulations to estimate aliasing and
benefit of "focal spot wobble"

<u>Task</u>	<u>Delivery</u>
Preliminary image quality assessment complete: LCD and aliasing artifacts	Q1
Creation of sCT geometries in VRAI	Q1
Experimental validation of VRAI Monte Carlo simulations	Q2
Generation of typical scatter profiles for wide area coverage	Q2
IQ tradeoff in sCT complete: LCD versus resolution	Q2
EDCT benefit in sCT	Q3
IQ impact of residual scatter assessed	Q4

Recon



Explore how to come close to the fundamental limits imposed by the laws of physics



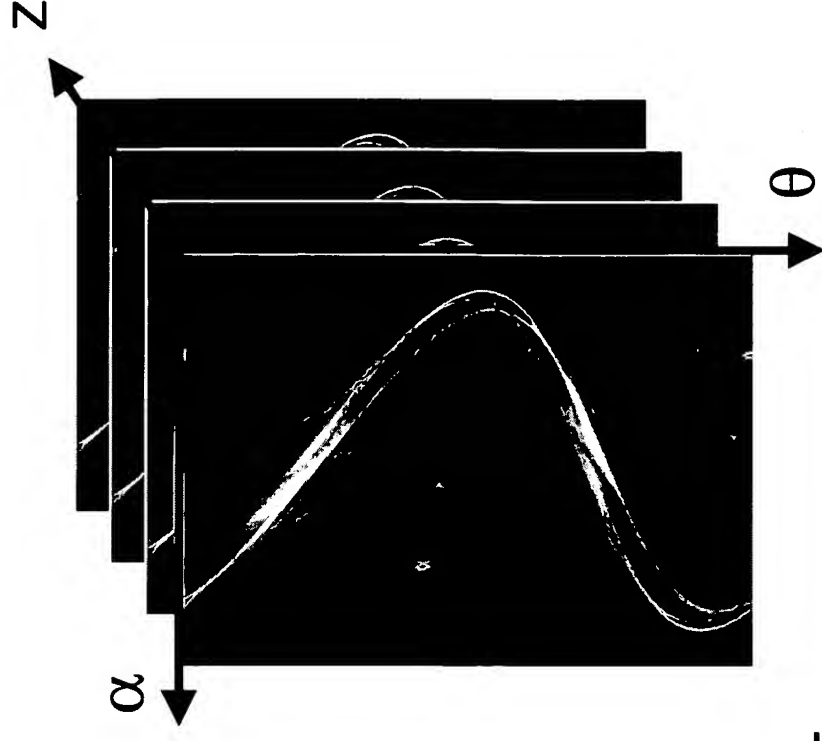
Recon methods will target high-noise environment

conventional :

- smooth along detector channels (α)
- tradeoff SNR with MTF

adaptive filtering :

- smooth in 3 dimensions (α, θ, z)
- locally adapt degree of smoothing to noise level
- improve SNR and maintain MTF



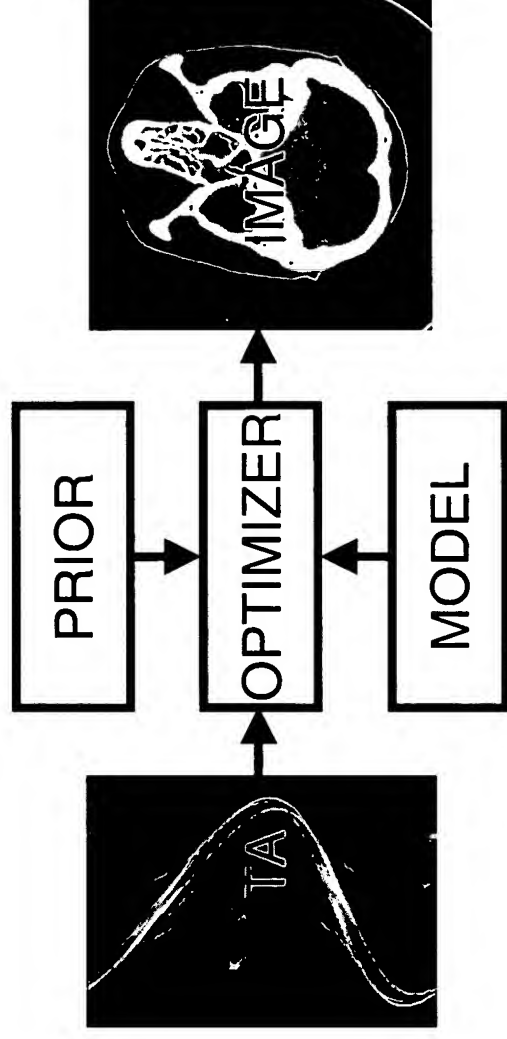
Benefit from non-uniformity of noise

Present :

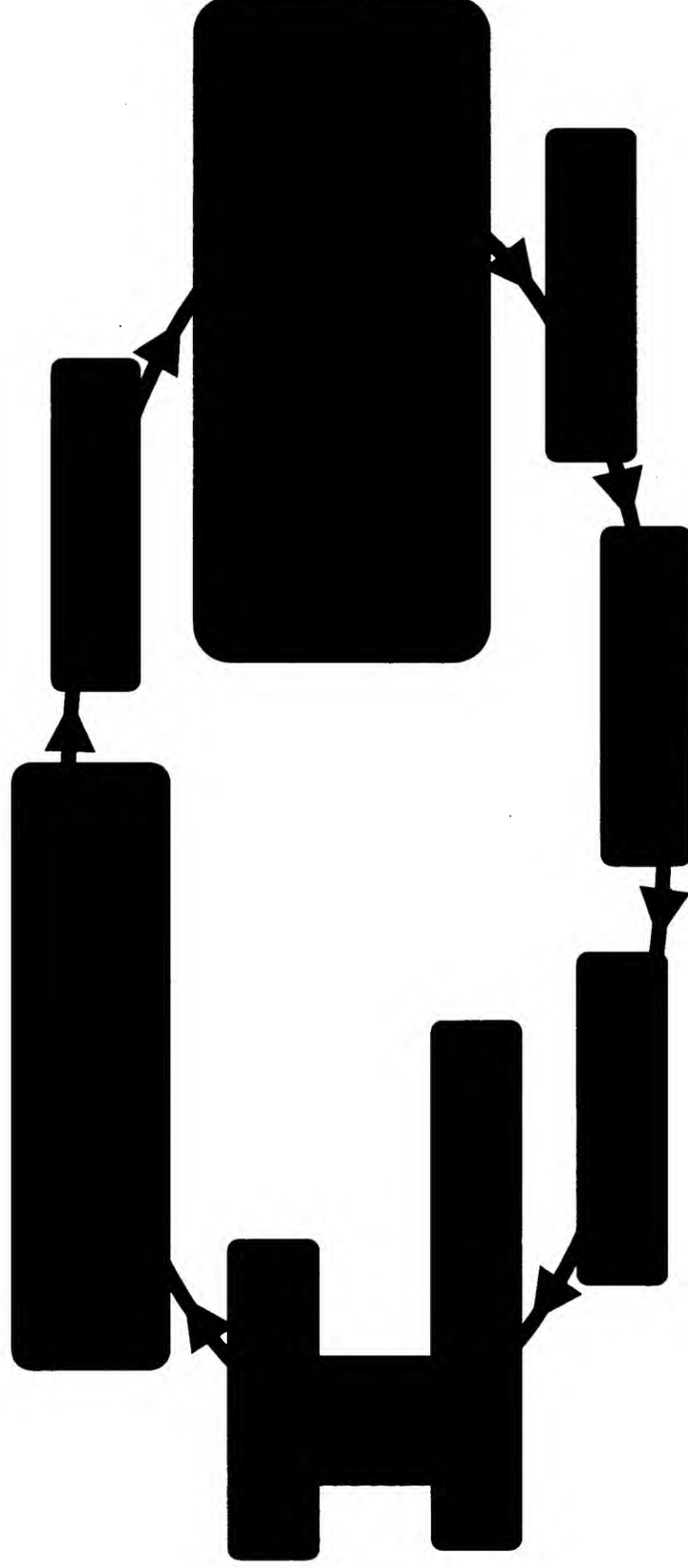
- ignore statistics of data
- ok for low-noise
- fast

Iterative reconstruction :

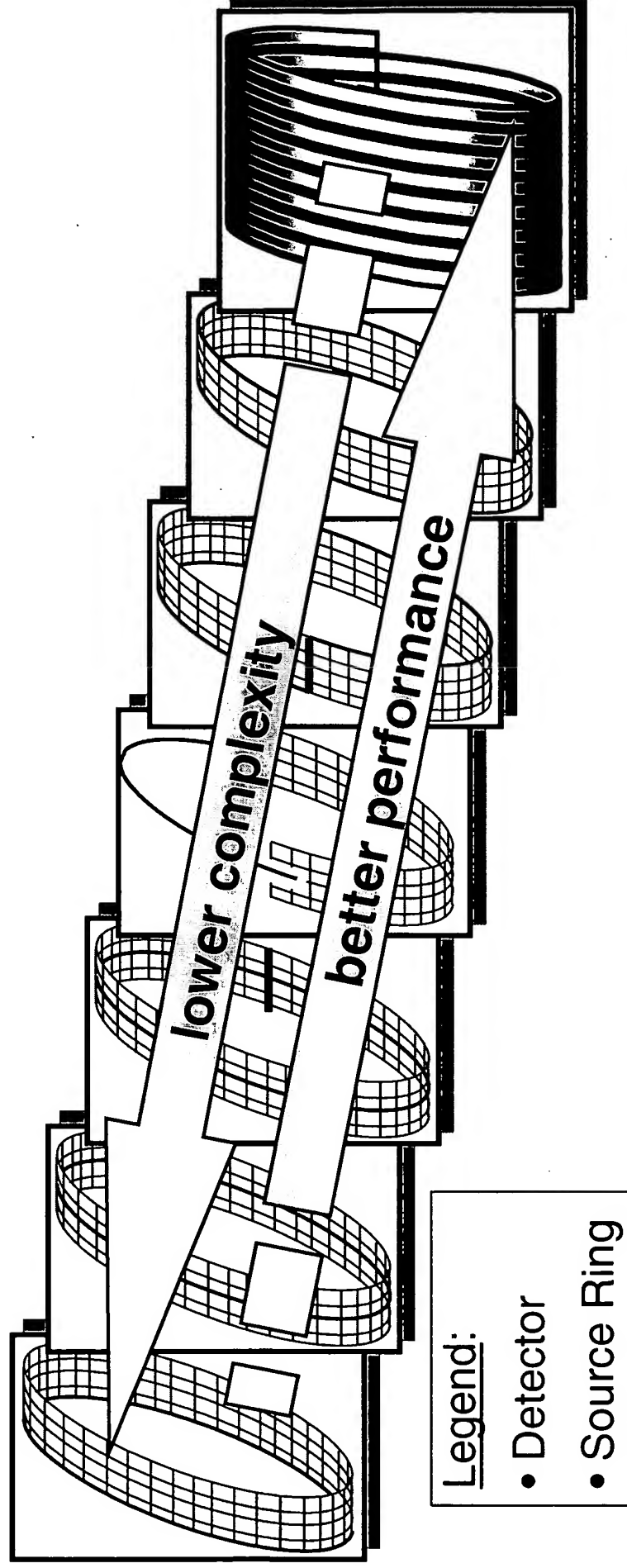
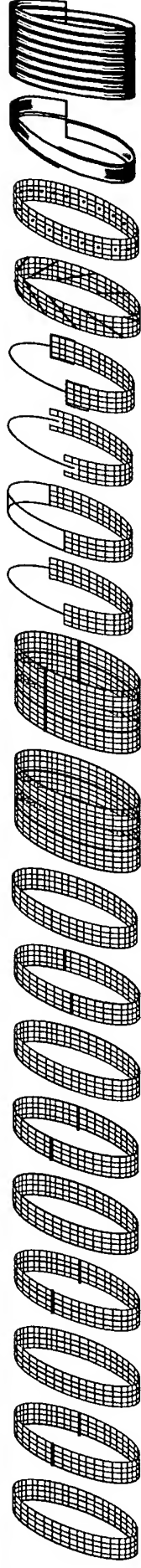
- use statistics of data
- 40% dose reduction (JBT)
- scan flexibility
- slow



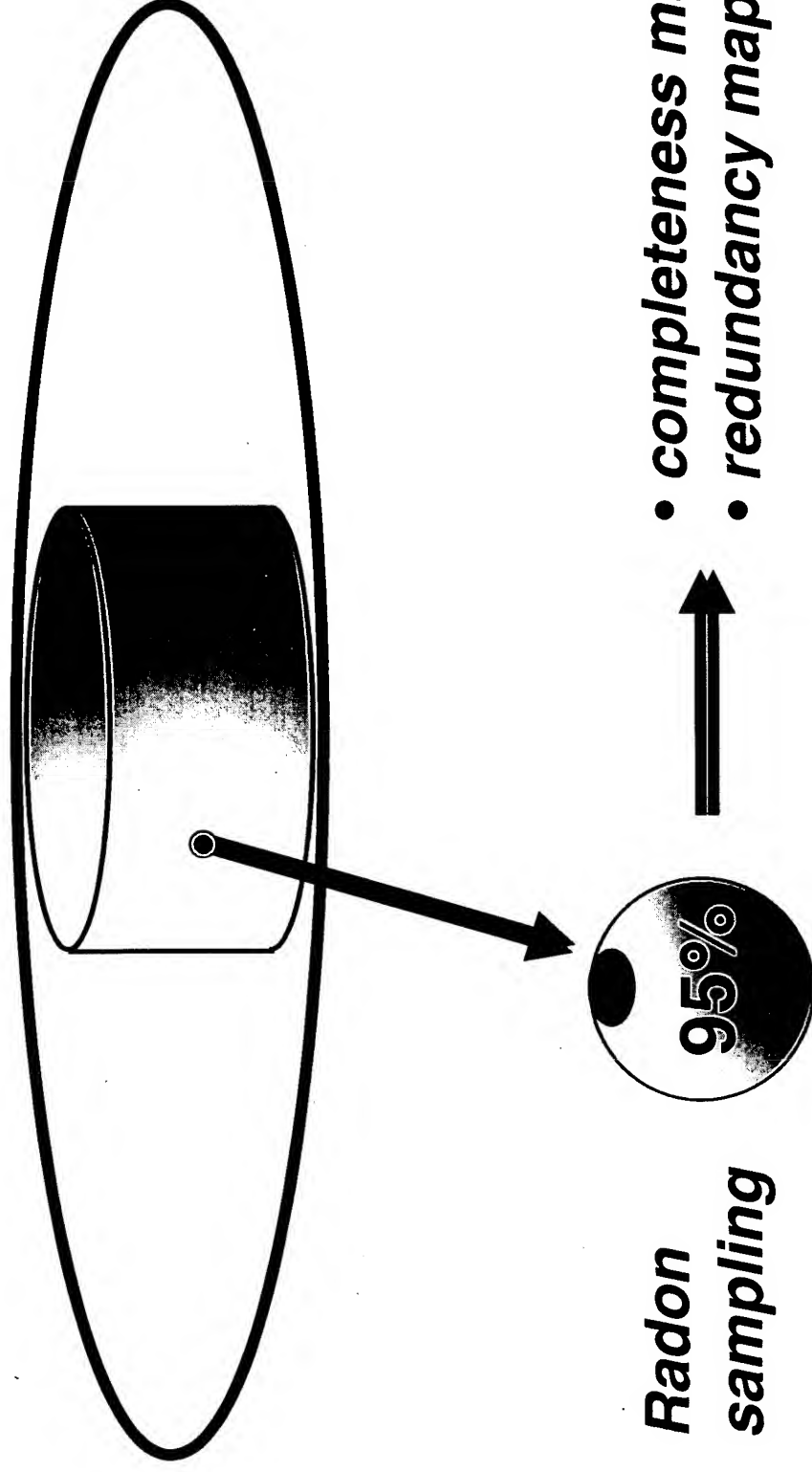
Statistical interpretation of statistical fluctuations



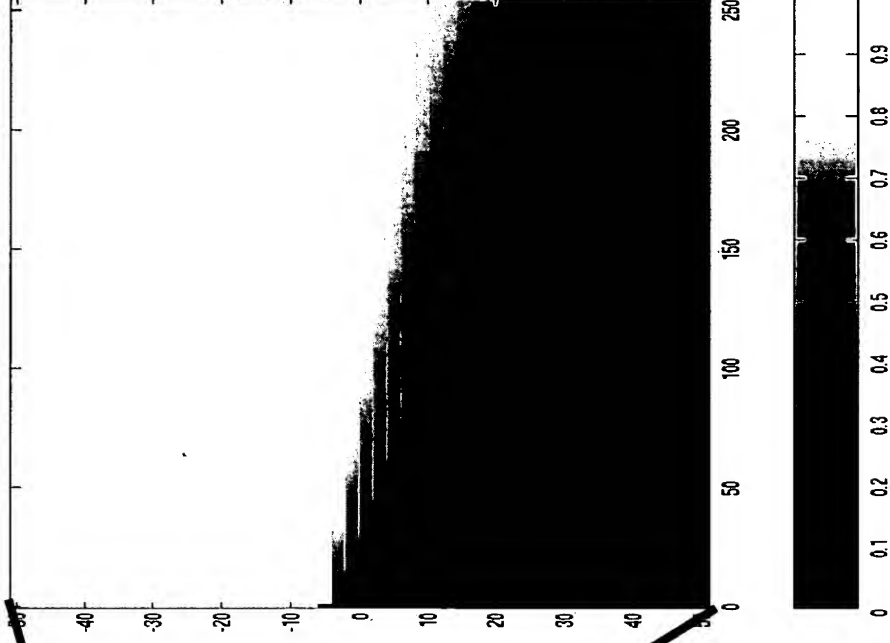
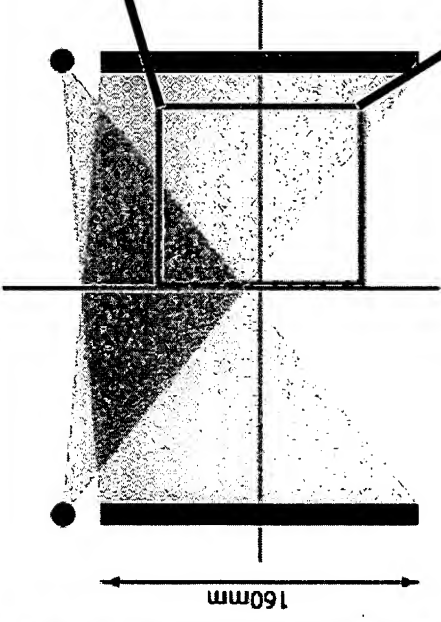
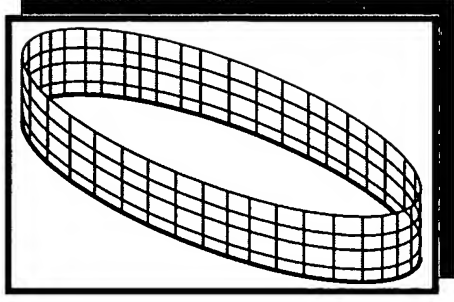
Start wide ... narrow down on optimal geometry



Tradeoff complexity with performance

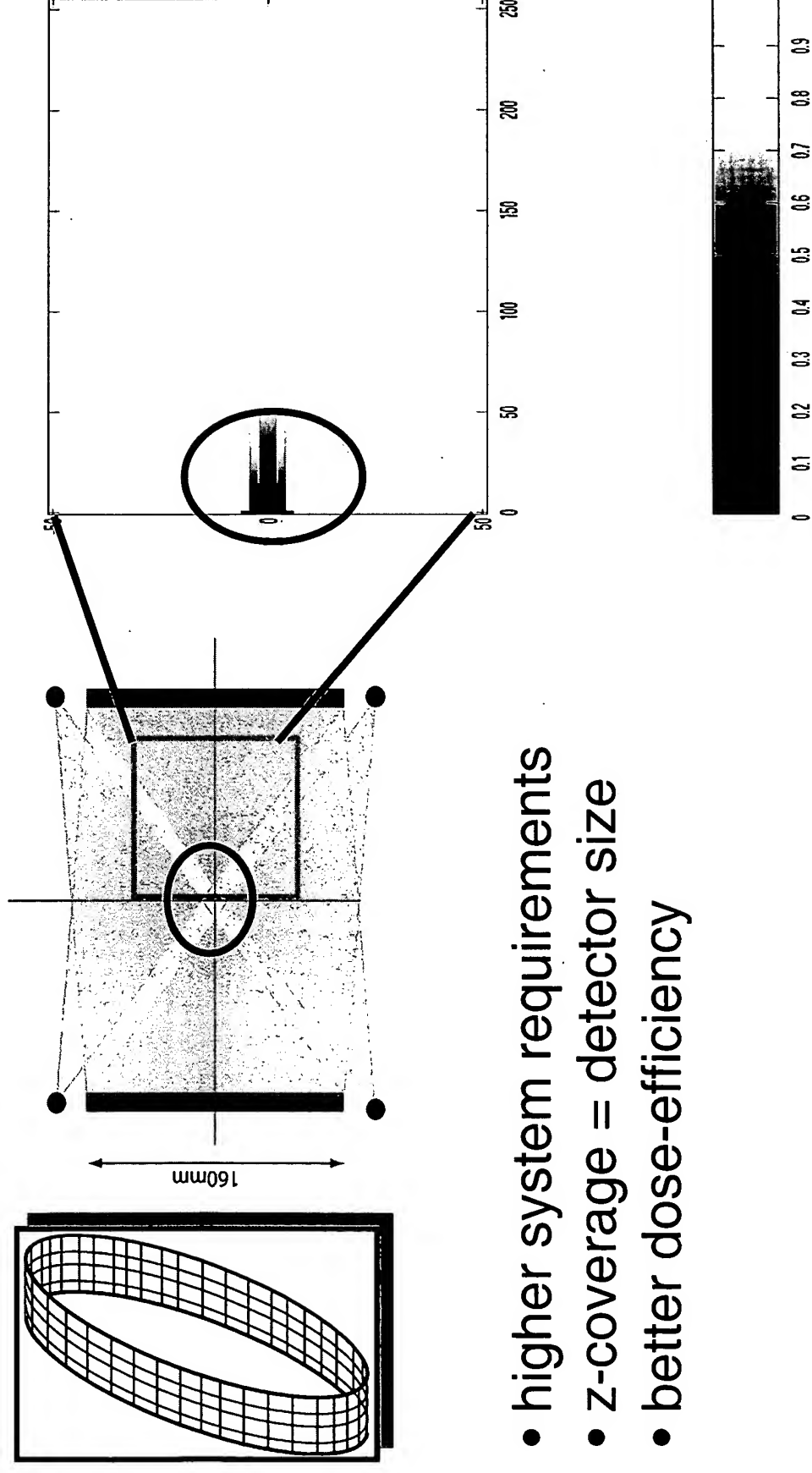


Local completeness measure – predict IQ



- low system requirements
- z-coverage = half detector size
- suboptimal dose-efficiency

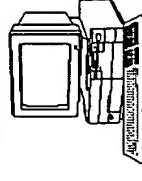
Single circle geometry is easy but inefficient



- higher system requirements
- z-coverage = detector size
- better dose-efficiency

Double circle geometry has better performance

RECON



①

Low-Dose investigations:

- Algorithm survey
- Generate simulation data
- Implement adaptive filtering
- Implement iterative recon
- Evaluate SNR benefits

1Q03

2Q03

2Q03

3Q03

4Q03



②

Geometric Evaluations:

- Exploration of geometries
- Numerical evaluation
- Simulation and reconstruction
- Evaluation & down-selection

1Q03

2Q03

4Q03

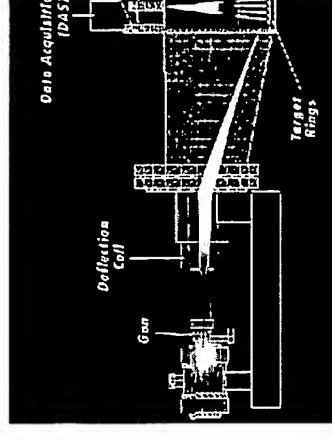
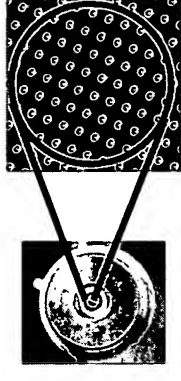
4Q03

***sCT is a great challenge – we will make it work !***

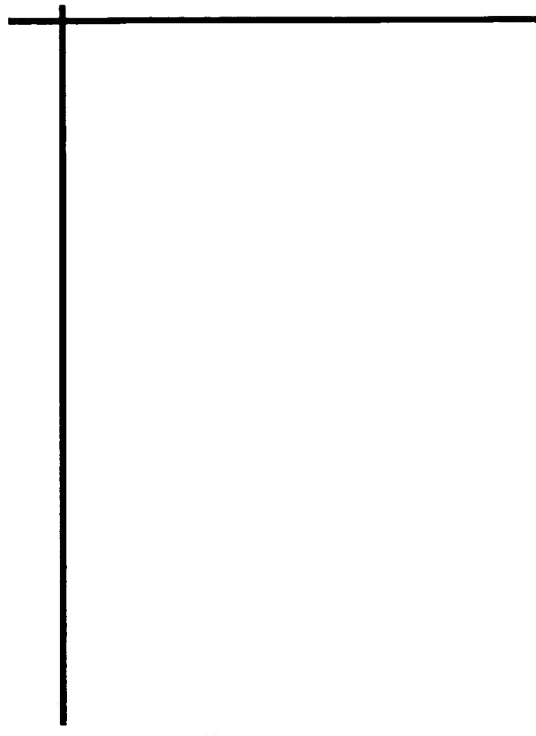
Appendix

Status

- **2001 Field Emitters (MGPD)**
 - Field emitter characterization (Spindt)
 - Key IP on distributed ring source
- **2001 Imatron acquisition**
 - Fast DAS, Ring target technology
- **2002 EDS proposal to TSA**
 - System concept & development timeline generated
- **2002 Breakthrough CT**
 - Single focal spot coverage limitations identified
 - High level system analysis - alternatives identified
 - Stanford Inverted Cone & UW Z-Scan projects begun
 - CT-CZT incentives established for Imarad
- **2002 Nanotechnology AT & NIST award**
 - Field emitter technology & partnering survey
 - NIST award for nanorod devices



Vision for new system materializing, good synergy with EBT



- At diagnostic x-ray energies, Compton scatter is very nearly elastic.
- 80keV gamma rays collide with 511keV electrons and the gamma ray loses almost no energy.
- For single-scatter, differentiating a scatter event that was deflected by one pixel would require differentiating a 79.99998 keV gamma ray from an 80.00000 keV one.

Detector

- High speed scintillator
- Energy discriminating detector

⇒ GE Imatron, LuTAG

⇒ 2003 CTE-funded project

DAS speed

- ~20x greater than Lightspeed
- Maintain IQ at high sample rates

⇒ GE Imatron

Cost

- Extended x-ray source
- Volume detector ring
- Data Acquisition System
- Energy Discrimination

⇒ Imatron Cost
Reduction

**With field emitter source technology, we could
build an sCT system!**



Appendix 2

Powell, William (GE, Research)

From: Leue, William M (GE, Research)
Sent: Friday, January 27, 2006 2:24 PM
To: Powell, William (GE, Research)
Subject: CAD integrated with recon for luggage screening

Importance: High

Bill,

The forwarded email is the earliest reference I can find: 3/28/2002. It encloses a document that Rick Avila wrote that includes words like '...tight integration between recon and CAD...'.
- Bill

-----Original Message-----

From: Avila, Ricardo S (CRD)
Sent: Thursday, March 28, 2002 8:49 AM
To: Leue, William M (CRD)
Subject: FW: CAD/Vis Section

Take a look at the CAD/Vis luggage screening document for some background. After yesterday's discussion with L3 we now have to revise the CAD section to not assume we will be doing full blown modeling based on shape (shoe, hard drive, etc.) I will explain later today.

- Rick

-----Original Message-----

From: Avila, Ricardo S (CRD)
Sent: Tuesday, March 26, 2002 5:08 PM
To: Mundy, Joseph (CRD); McCulloch, Colin (CRD); Kaucic, Robert A (CRD); Lorensen, William E (CRD); Kelliher, Timothy P (CRD)
Cc: Grabb, Mark L (CRD)
Subject: FW: CAD/Vis Section

Here is the CAD/Vis part of the EDS long term proposal (5 years). Please give it a read and mark up changes in red.

We will also need to write up a short term CAD/Vis proposal that I am now told will be for 3 years (not one year as we originally thought).

- Rick

-----Original Message-----

From: Avila, Ricardo S (CRD)
Sent: Friday, March 22, 2002 3:07 PM
To: 'jerrybrooks@pagesplusinc.com'; Hopkins, Forrest (CRD)
Cc: Walter, Deborah (CRD)
Subject: CAD/Vis Section

Here is the final CAD/Vis input for our 3pm deadline.

I will also put this into the quickplace under EDS - Long Term.

Let me know if you see an issue with it.



5-CADVisProposal
3_22_02.doc

Ricardo S. Avila

Clinical Applications and CAD Project Manager
Imaging Technologies

GE Global Research Center	Email: avila@crd.ge.com
1 Research Circle, KW C220A	Phone: (518) 387-6632, 8*833-6632
Niskayuna, NY 12309	Fax: (518) 387-6981

CAD/Visualization Technical Discussion and Approach

1.0 CAD/Visualization System Architecture

The next generation of Explosive Detection Systems must leverage and globally optimize across a variety of information, threat sensing, and baggage handling subsystems. The information obtained from these subsystems will be processed by state-of-the-art Computer Aided Detection (CAD) and Visualization subsystems. The main goal of the CAD and Visualization Subsystems is to achieve a high baggage throughput, a high detection rate (sensitivity), and a low false alarm rate (1-specificity) with as little human assistance as possible. In addition, we seek an EDS design that can easily and appropriately scale to the capacity, and level of threat measurement and processing required at an individual airport given rapidly changing security concerns.

Achieving these goals for an EDS with a 1500 bag/hour throughput translates into an average CAD processing time of approximately 2 seconds per scanned bag. A high throughput and automated EDS that achieves high detection accuracy will need to:

- (1) Consider as much salient information as is available on the passenger and baggage in question. Significant gains are possible leveraging a dual energy CT acquisition system and an ETD monitor.
- (2) Tightly couple and pipeline the CT reconstruction and CAD subsystems in order to streamline data processing and automatically obtain the highest possible image quality when the level of threat is found to be high.
- (3) Analyze the contents of each bag with state-of-the-art Computer Aided Detection algorithms that comprehensively model False Alarm objects as well as explosive devices and optimally reason with all of the information available.
- (4) Provide all relevant information from all subsystems to a highly automated visualization application console for a final digital review of suspicious baggage by a human operator.
- (5) Utilize a powerful, cost effective, and scalable computing engine that adaptively allocates processing power to the level of threat.

Figure 1 illustrates the flow of baggage and information across such a system. Those elements shown in green can be considered optional modules which when added to the EDS would significantly improve detection rate and reduce the false positive rate.

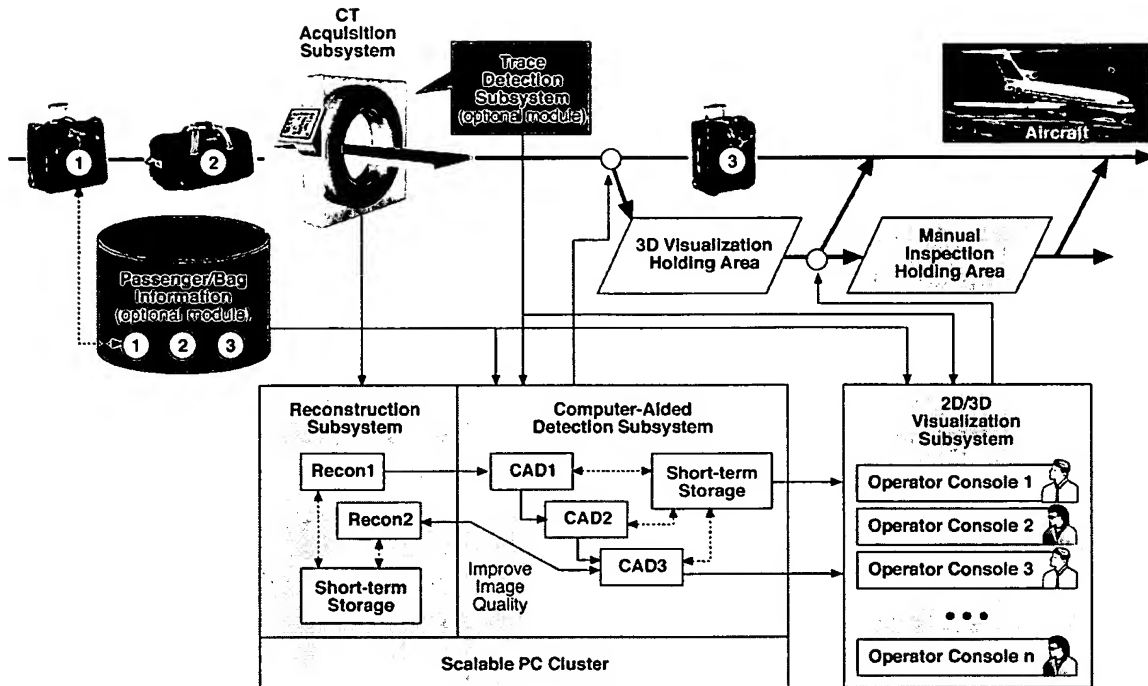


Figure 1: A highly integrated Reconstruction, CAD, and Visualization Architecture

The system starts with a high throughput stream of baggage flowing into the CT acquisition subsystem. The acquired projection data is incrementally transferred to the reconstruction subsystem for processing into a 3D CT representation. The 3D representation will ideally consist of two scalar CT values representing two independent energy levels. Each reconstructed slice is incrementally then sent to the CAD subsystem for automatic threat detection. If passenger and flight information is available for each bag then this will also be provided to the CAD subsystem. An optional ETD subsystem may also scan the bag for trace evidence of explosives. The ETD information including the level of threat and the chemical composition of the sampled threat will also be provided to the CAD subsystem. The CAD subsystem performs advanced image analysis on the 3D CT scans of the luggage taking into account all of the information provided on the passenger, the flight, and the sensors applied to the baggage. This would allow the EDS to automatically customize the level and type of scrutiny placed on an individual bag based on all of the information available.

The Reconstruction and CAD subsystems are tightly coupled allowing for additional targeted reconstructions to be automatically performed on baggage if the CAD subsystem requires higher quality slice data to make a critical decision. Both subsystems will utilize a scalable cluster of standard PC processing units. This novel architecture allows the Reconstruction and CAD subsystems to dynamically adjust computational loading for each piece of luggage. The reconstructed images will then be sent to a hierarchical CAD subsystem consisting of three levels of CAD processing. Should the CAD subsystem find that the bag is a significant threat to the safe operation of the aircraft it must send a signal to have the bag automatically pulled from the baggage stream and held for additional scrutiny. The low percentage of bag scans that are considered suspicious after CAD

processing will be analyzed by human operators utilizing advanced imaging tools in the Visualization Subsystem. This last level of digital inspection is intended to minimize the number of bags that must be manually opened and inspected. All of the information acquired and computed for the bag will then be sent to a Visualization subsystem where operators will have advanced 2D and 3D tools for performing a virtual inspection of the suspicious bag. If after operator analysis the bag is no longer considered a threat it will be placed back in the normal baggage stream. Otherwise it will be sent to a holding area for manual inspection. The performance of the entire EDS will be optimized in order to achieve the best combination of operations cost and accuracy of the system.

1.1 General CAD Approach

GE Global Research has developed a general approach to the Computer Aided Detection (CAD) of objects based on the use of mathematical models. These models represent various stages of representation for CT images of a subject. At present, the approach is based on three stages of representation and is being applied toward the early detection of lung cancer in CT images. The models are currently directed at the representation of the lung in support of lung cancer detection in CT images, however the approach can apply to any detection application.

Signal models – The first stage of representation is the signal formation process. In this example, the images are formed by X-ray computer tomography (X-ray CT). The signal models represent the blurring and noise process inherent in the CT image formation process. These models also support the detection of primitive events in the image such as linear features or discontinuities in density. These primitive features form the basis for later stages of representation. These signal models utilize detailed knowledge of the physics of image formation and the resulting signal properties.

Shape models – The next stage of representation captures the appearance of features in the image in terms of their intensity and shape. This representation provides an elementary vocabulary for describing three dimensional structures and to group the detections made at the signal level. The role of these representations is to explain the intensity or density of groups of pixels in terms of perceptual units.

Object models - The last stage of representation is in terms of physical object concepts. The earlier representations are further grouped and parameterized in terms of higher level object units. For example, a sheet object along with a thin cylindrical wire can be interpreted as an explosive threat with appropriate constraints on the density and mass that would be consistent with explosive manufacturing technology.

Model Selection – At any stage of representation there are a number of models that might provide an interpretation of the underlying image or group of features. It is necessary to have a unified framework for model selection. In our current approach we use Bayesian statistical methods to select the model that provides the most probable interpretation of the data, given prior constraints on the model. The models are viewed as competing for the best interpretation of the data. In this approach, there is no need for

pattern recognition or neural net classifiers since the models carry their own classification mechanisms that are particularly tailored to the data representation.

Figure 1 demonstrates our early work in automated detection of lung cancer in low dose CT scans. The left image (a) demonstrates the ability to automatically detect the outer lung boundary in CT scans. The middle image (b) shows the ability to track vascular structure (blue) as well as candidate regions in the image that may indicate the early presentation of lung cancer (green). The right image (c) is a magnification of detection results centered on a suspicious lung lesion.

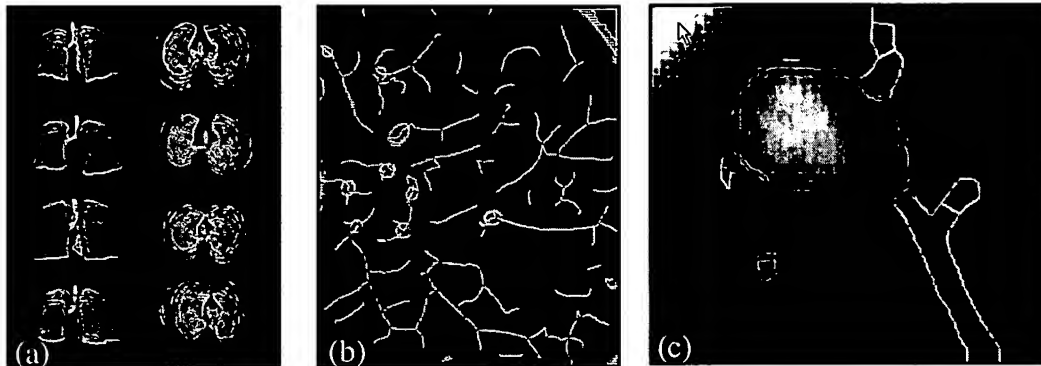


Figure 1 Examples from our current work on lung cancer.

GE's Complete knowledge of medical scanner acquisition and reconstruction techniques will allow us implement carefully engineered signal models that avoid the need for learning or training. The models can be adapted by known acquisition parameters or from data from a single phantom. At the same time, our sound mathematical modeling effort will enable quantitative analysis of the effect of acquisition protocols on detection performance. For example, in acquisition based on X-rays, it is necessary to trade off dose against detection sensitivity.

1.2 CAD Subsystem

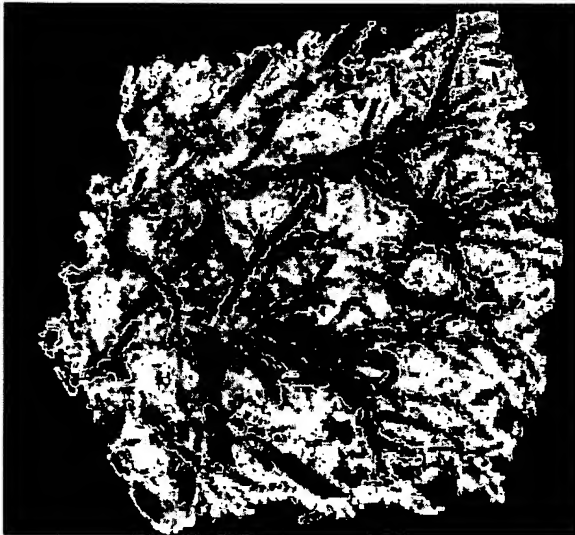
To achieve our three goals of rapid luggage throughput, extremely high sensitivity for explosive detection, and a low false positive rate we propose a hierarchical architecture for Computer Aided Detection (CAD). Our system will consist of several levels of processing. We rule out clearly nonthreatening luggage early in the hierarchy with a minimum amount of processing. In subsequent levels, we employ an amount of processing which is commensurate with the perceived level of threat. In this way, for a given luggage throughput specification, our ability to rule out luggage through coarser image processing methods allows us more processing time for finer detection techniques. Each processing level will maintain a high specified detection sensitivity level.

We propose a three level CAD system. Each level of processing will be based on the same overall *Model-Based Detection* framework, where the sophistication of the models and data increases as we descend the hierarchy. We define Model-Based Detection as the identification and classification of objects through the use of detailed models fusing CT

density, morphology, and domain knowledge quantified in the form of prior probability distributions. These models can be further supplemented with other non-image information to increase detection performance.

The aim of the first level of detection is to rapidly screen baggage that can be ruled out with computationally inexpensive image processing methods. The result of this first processing level is high sensitivity and relatively low specificity. For instance, large masses can be formed by connecting regions of similar CT density to form geometric structures. Baggage scans containing masses exhibiting properties consistent with explosive materials are passed on to the second level of processing, while those bags not exhibiting such properties require no further analysis. Sensitivity will be significantly increased at this and later detection processing levels when dual X-ray energy discrimination is achievable. We plan to assign a significant amount of effort to this task.

In the second level of detection processing, more computational resources are focused on the potentially suspicious luggage scans to achieve higher specificity without sacrificing sensitivity. Here, more detailed differential geometry-based segmentation can be used to permit finer identification of objects. In our many years of experience developing automated detection systems for intelligence, military, and medical applications, we have found that differential geometric image analysis methods provide a robust and highly sensitive framework for image quantification. For example, the three-dimensional Hessian matrix (the 3x3 matrix of spatial second order partial derivatives) gives several measures for quantifying object shape from intensity profiles. Figure 3 gives a volume rendering of the vessel network in a CT lung scan. In this application, we segmented the lung's vessel network to improve cancer detection. Here we plot the square root of the product of the first two Hessian eigenvectors in shades of red. This measure is designed to highlight regions of cylindrical (vessel-like) intensity profiles, and it performs extremely well in this application. This has direct application to explosives detection because a variety of different canonical object shapes (for instance planar or sheet-like explosives) can be identified in the CT imagery through properly chosen functions of differential geometric operators.



$$\mathbf{V}^t \mathbf{H} \mathbf{V} = \begin{bmatrix} \lambda_0 & 0 & 0 \\ 0 & \lambda_1 & 0 \\ 0 & 0 & \lambda_2 \end{bmatrix}$$

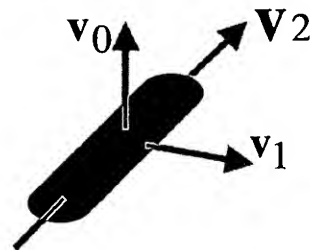


Figure 3: Three-dimensional volume rendering of the vessel network in a CT lung scan. The square root of the product of the first two eigenvalues of the 3d Hessian matrix (H) is given in red. Each column of the matrix V contains an eigenvector, v_0 , v_1 , and v_2 which are oriented relative to a cylinder as shown in the right panel.

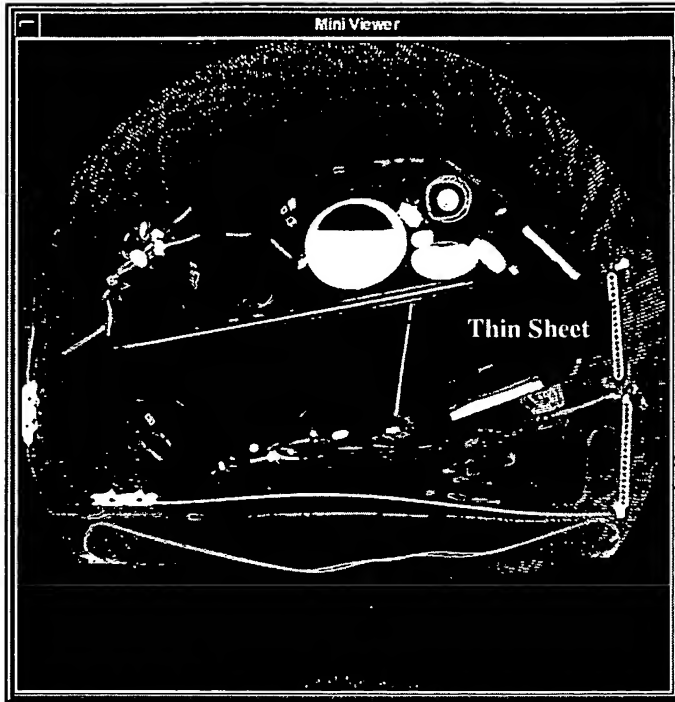


Figure 4: CT scan of a piece of luggage containing a variety of objects including a thin sheet.

A key advantage we have at GE when designing segmentation and detection algorithms is our ability to use comprehensive knowledge of the point-spread function characteristics of the CT scanner to aid precise identification of objects. For example, further processing of the lung scan given above was performed to accurately measure the fine structure around air bronchioles. These tiny airways have wall thicknesses on the order of the resolution of the CT scanner. We must therefore carefully use the scanner specifications when making these subpixel measurements. The top panel of Figure 4 gives a graphical representation of our bronchiole wall CT profile model. This model involves a convolution of an anatomical bronchiole model with the known scanner point-spread function to generate a predicted CT intensity profile. The bottom panel shows our detections of bronchioles in a sample image. The wall thickness is measured by deconvolving the scanner point spread function from the anatomical model and estimating the model's thickness parameter via statistical maximum likelihood estimation.

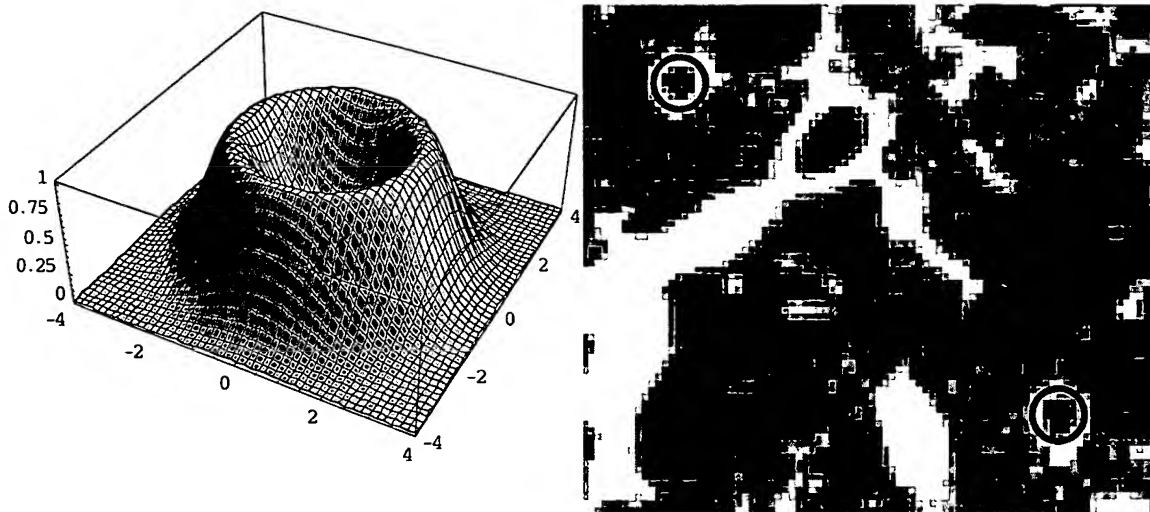


Figure 5: Bronchiole wall detection and measurement. The left panel gives the convolution of anatomical model with the scanner point spread function. The right panel gives an example lung scan with two automatic detections highlighted.

Detailed probabilistic models will be developed of both threat and non-threat objects. These models will be constructed from a collection (database) of example imagery of explosive materials and confounding objects. We will classify segmented objects (called “model matching” in our task list) by incorporating features obtained from the imagery, chemical trace analysis, and passenger and flight information using pattern recognition methods. In our experience, we have found optimal Bayesian classification methods to be most powerful in discerning targets of interest (e.g. explosives) from confounding objects (those articles expected in normal luggage). This type of classification proceeds by first assigning prior probability distributions on object models using expert knowledge on target characteristics like CT signature, morphology, and any available non-image data. Next, we combine these models with the incoming data on a particular bag through strict Bayesian probability calculations to report an overall probability of explosives threat. Bags exhibiting a specified minimum threat probability are deemed suitable for further scrutiny.

Baggage not ruled out as nonthreatening continues to level three detection. Objects deemed suspicious by level two processing are reconstructed at a higher resolution using the reconstruction hardware. In addition, reconstruction artifacts due to baggage hardware identified in level two are eliminated. Classification is then performed on this higher resolution, artifact-free imagery resulting in higher classification rates of suspicious objects. This image reconstruction feedback loop can be implemented iteratively, by continuously identifying suspicious objects through Bayesian classification and increasing CT resolution at those object locations. In this way we constantly optimize our certainty (probability) of candidate object model representations.

Finally, bags that exhibit a high threat probability by the hierarchical CAD system and therefore are deemed suspicious are sent to a visualization workstation for interactive human review. A key strength of our model-based processing pipeline is that the salient

detection probabilities and other segmentation measures are sent to the visualization workstation to automate and guide interactive inspection.

For development of sensitive and robust CAD systems, a large database of imagery and metadata will be required. Ultimately this database will contain labeled imagery of threats and non-threats from the final production CT hardware with chemical trace and other non-image data. Initially, however, labeled imagery from currently available CT systems will be acquired for CAD development. This task will require detailed work by CT technicians and screening experts to formulate a representative database of the full range of luggage scenarios.

1.3 Detection System Validation

GE Global Research has developed a fully automated infrastructure for detection algorithm testing and validation consisting of several components. Software quality is monitored through nightly builds and automatic algorithm tests. A test-bed cluster of 92 Pentium class CPU's is managed by a web-enabled interface. This facilitates algorithm developers to design experiments which measure performance of proposed algorithms on a large database of images with minimal interaction. We quantify algorithm performance statistically using general Receiver Operating Characteristic Curves (ROC) and other performance summary measures. ROC curves are effective at showing graphically the trade-off between CAD system sensitivity and specificity. Also, ROC analysis allows us to statistically compare the performance of two candidate detection systems to determine if perceived performance differences are real or merely due to noise in the test image database.

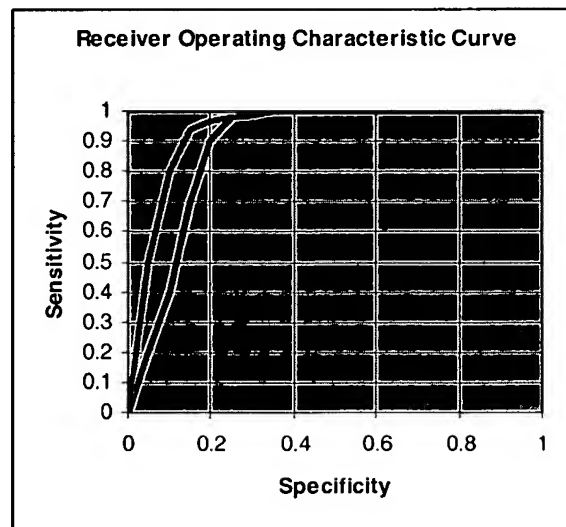


Figure 6: An example receiver operating characteristic curve comparing two CAD algorithms. The algorithm plotted in pink gives consistently higher detection sensitivity for a range of false positive rates (specificity).

The significant time GE has devoted to this validation infrastructure gives us a large head-start to begin testing detection methods at the very beginning of an awarded contract.

1.4 Visualization Subsystem

Visualization is the process of transforming and combining data into forms that are suitable for presentation to a human. In the baggage inspection system, the visualization station is the vehicle for displaying the fused information from various sensor and analysis subsystems. The system serves as the interface between the human operator, the imaging equipment and the segmentation and detection algorithms. The major challenges of the visualization system revolve around the baggage system's high throughput requirement. To achieve the desired throughput the visualization must be able to give the operator an initial pass/fail indication at a glance. For those that are indicated as failing, the visualization must be tuned to display the reasons for failure and provide a means for further interrogation. This interrogation must be intuitive in its application and self-guiding such that the system operator does not spend time interpreting the unprocessed CT imagery. Thus speed, rapid navigation of the 3D volume, fusion of acquired and derived information, limited user input and interaction become the driving requirements for the system operational concept. To meet these requirements, we propose to apply existing and develop new visualization algorithms augmented by automated parameter selection and adaptive visualization protocols. These techniques will be provided in a baggage visualization toolkit that is designed to achieve these requirements – and be flexible enough to continuously improve as new techniques and customer-specified display platforms evolve.

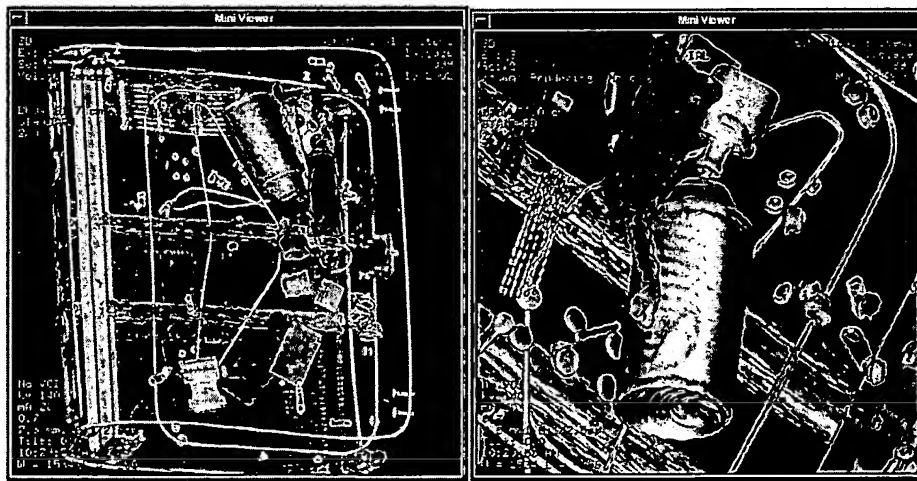


Figure 7: Shaded volume rendering of multiple objects in baggage.

The acquired stack of CT slices can be visualized all at once using volume rendering techniques. Volume rendering displays "projections" of the slices. These projections are synthesized by passing rays through the volume elements (voxels) of the data. The projection can simulate physical properties such as x-ray attenuation. However, many other projections are possible by remapping the sampled values through "transfer functions." The transfer functions convert the samples and other local information into intensities, colors and opacities. Through appropriate transfer function design, CT data can be transformed into displays that highlight various materials as shown in **Figure 7**.

However, as with two-dimensional displays, transfer function design is too difficult and time-consuming to be used in a high throughput application. The degree of difficulty is potentially higher in baggage systems than in medical applications since the range of materials in a suitcase is so vast.

The main focus of the volume display is performance and automation. Performance of the volume rendering has a significant impact on system throughput. We will develop techniques that produce the volume rendering as soon as become available from the acquisition and detection subsystems. This incremental volume rendering approach permits overlapping the volume presentation with reconstruction and analysis. Once the final slices are available the rendering is complete. We have successfully deployed real-time incremental volume rendering and analysis on our Lightspeed helical CT system. We will also investigate other volume acceleration techniques including hardware acceleration using commodity graphics boards and distributed rendering across multiple commodity workstation systems.

Automation impacts operator performance and effectiveness. We propose to investigate, invent and implement automated transfer function technology that will highlight all important structures and materials found in the baggage. These novel techniques will produce transfer functions that map single or dual energy intensities and image gradient information into effective presentations of significant objects in the baggage. The results of the detection and segmentation algorithms will be used to guide the selection and parameterization of the transfer functions. For example, we have already demonstrated techniques that use volume segmentation masks to apply multiple transfer functions within a volume. This mechanism provides visual emphasis to the results created by the detection subsystem.

Detection and segmentation results identify regions of the CT data that warrant further processing. Typically, segmentation algorithms produce labels that identify a voxel as being a member of a set of possible objects. Detection algorithms produce a wealth of quantitative information about regions of the volume. The detection results may be voxel labels but are more often defined by line segments or surfaces.

We propose to integrate (or fuse) the region and surface detection results with the intensities in the CT volume. The detection results will be used to emphasize or de-emphasize regions of the volume displays. For example, the results of segmentation may identify regions that are known to be non-threats. The visualization system can use this information to remove those structures from the presentation. We have demonstrated this capability in a medical application that removes the bone from CT abdominal studies so that the vascular structure is easy to visualize.

Simulation results include geometric models of baggage and baggage contents as well as volumetric models of these items and explosive materials. These models can be registered with the scanner results to help operators perform visual comparisons with known threats and non-threats. For example, a volume model of a particular brand of suitcase can be juxtaposed with the scans of the passenger's luggage. Suspicious

intensities in or around the plastic wheels can be visually compared with the known scans of the reference luggage. We propose to provide registration techniques that will automatically align simulation models with the acquired data.

The visualization algorithms will be encapsulated in a toolkit that can operate on both Unix/Linux and Windows platforms. This approach permits the integration of the techniques into a various display systems. The architecture of the toolkit will permit the addition of new visualization techniques as they are discovered.

1.5 Development Plan

Task 1.1 - Establish Database

We will develop a development database of CT scans for CAD and Visualization algorithm development and validation. A large number of scans must be acquired to obtain statistically significant validation results. The scans must contain objects that represent the full population of true explosive devices as well the many objects that may cause a false alarm. In addition the development of phantoms will be required. This task will be frontloaded to provide the algorithm developers with sufficient data to begin designing algorithms as early as possible.

Task 1.2 - Scanner Modeling

This task will focus on obtaining a thorough understanding of the CT scanner point spread function and all factors that will influence it. In particular the point spread function of the scanner must be well understood in order to achieve optimal detection accuracy.

Task 1.3 – Object Segmentation

This work will center on the analysis on the generation of a fully automatic and three-dimensional segmentation of the 3D CT scan using 3D edge detection methods. These regions will be topologically consistent and created incrementally as data is provided to the CAD subsystem.

Task 1.4 – Geometric Representations

The result of object segmentation will be analyzed to understand the 3D geometry of the objects in the CT scan. These techniques must be resilient to significant metal artifact and low contrast scanning issues.

Task 1.5 – Threat/Non-Threat Model Development

Geometric models are developed into precise mathematical models capturing the variation within model populations. Significant interaction time will take place between algorithm developers and luggage screening and explosives technology

personnel to arrive at the best possible models. A large number of threat and non-threat models will need to be developed to arrive at high detection sensitivity and specificity. Methods must be developed to determine when it is appropriate to request a higher quality reconstruction.

Task 1.6 – Model Matching

The decision making framework for selecting the most probable model will be developed. This framework must support the hierarchical nature of the decision making process. The framework will be flexible in that it will allow for updates to the number and types of models as new threats and false alarms are discovered.

Task 1.7 – Hierarchical Detection Architecture

The computing platform, high level application and data transfer required to support a hierarchical CAD architecture will be developed. This system must be able to dynamically adjust resources as the level of threat changes.

Task 1.8 – Optimization of Performance

Achieving a CAD processing rate of approximately 2 seconds per bag will require extensive performance optimization on algorithms and data transport through the system.

Task 1.9 – Energy Discrimination Modeling

The entire CAD processing architecture will be extended to support dual energy discrimination. Since some EDS systems will not have this capability the CAD subsystem must be able to leverage the extra energy data when it is available.

Task 1.10 – 3D Presentation

2D and 3D rendering techniques will be developed in the context of operator decision making ability. Volume rendering algorithms will be developed that are capable of displaying multiple scalars fields (dual energy) for maximum operator understanding. Algorithms will be developed that automate the generation of visualization settings. A luggage visualization toolkit will be developed that provides these techniques in a form that is easy to incorporate into applications.

Task 1.11 – Visualization Graphics Hardware

Advances in graphics hardware will be leveraged to allow the Visualization console operator to manipulate and visualize CT scans in real-time.

1.6 Milestones and Gaant Chart

Program Activities	Y1				Y2				Y3				Y4				Y5			
	1	2	3	4	1	2	3	4	1	2	3	4	1	2	3	4	1	2	3	4
Task 1 CAD and Image Quality.																				
1.1 Establish database.																				
1.2 Scanner modeling.																				
1.3 Segmentation.																				
1.4 Geometric representations.																				
1.5 Threat/non-threat model development.																				
1.6 Model matching.																				
1.7 Terraced detection architecture.																				
1.8 Optimization of performance.																				
1.9 Energy discrimination modeling.																				
1.10 3D presentation.																				
1.11 Visualization graphics hardware.																				
<i>Milestone: 35% false positive rate (coinciding with first image) achieved.</i>																				
<i>Milestone: Less than 20% false positive rate achieved.</i>																				
Task 2 Program Management																				
Quarterly reports	▽	▽	▽	▽	▽	▽	▽	▽	▽	▽	▽	▽	▽	▽	▽	▽	▽	▽	▽	▽
Annual reports																				
Final report.																				▽

Key: ▽ = Deliverables/Reports, ◆ = Milestones

Appl. No. 10/743,195

Reply to Office action of November 15, 2005

139681-2

Appendix 3

GEVTK/Segmentation/vtkImageHessianResponse.cxx - view - 1.26 - Microsoft Internet Explorer

File Edit View Favorites Tools Help

Back Forward Stop Search Favorites Media Print View Source

Address <https://openge.ge.com/cgi-bin/cvsweb.cgi/GEVTK/Segmentation/vtkImageHessianResponse.cxx?rev=1.26&content-type=text/x-cvsweb-markup&cvsroot>

Go file Search Search 101 blocked View Check Available AutoFill Options

Return to [vtkImageHessianResponse.cxx CVS log](#)

File: [\[hccvroot\] / GEVTK / Segmentation / vtkImageHessianResponse.cxx \(download\)](#)

Revision 1.26, Fri Dec 27 08:54:11 2002 EST (2 years, 9 months ago) by *lorensen*

Branch: MAIN

Changes since 1.25: +5 -4 lines

ERR: vtk include madness.

/*****

```
Program:      Visualization Toolkit
Module:       $RCSfile: vtkImageHessianResponse.cxx,v $
Language:     C++
Date:        $Date: 2002/12/27 13:54:11 $
Version:     $Revision: 1.26 $
```

*****/

```
#include "vtkImageData.h"
```

```
#include "vtkImageHessianResponse.h"
```

Part of CVS source code repository commit log, showing a commit of the source code for "vtkImageHessianResponse.cxx", the implementation of the Hessian filter. The commit date is December 27, 2002.

Appendix 4

Powell, William (GE, Research)

From: Leue, William M (Research)
Sent: Thursday, January 23, 2003 2:56 PM
To: Avila, Ricardo S (Research); Gorman, William (Research); Hammond, Christopher R (Research); Kaucic, Robert A (Research); Kelliher, Timothy P (Research)
Subject: Corrected version of Final Report sent to L-3

Tim and I worked with some data supplied by Eric Cardinal of L-3 to finally resolve the preclassifier detection rate puzzle. I have sent a corrected version of the Final Report to L-3. So far as I am concerned, this action finishes ALL of our deliverables for the 2002 project.

In my email that accompanied the report, I said:

"In my opinion, the broad conclusions of the report do not change much. The Vector Hessian (VHess) algorithm has detection rates that are comparable to but slightly lower than the EDS version 104 software. The VHess algorithm also generates many fewer total sheet objects than does EDS104. This fact should make it easier for the classifier to separate true detections from false alarms. However, writing a classifier that matches the output of VHess was outside the scope of this project, and so realizing the potential performance of the VHess algorithms will require further work."

I don't want to bomb your mailboxes, but you can get a copy of corrected report from the CVS repository:
l3det/docs/Final_report_v2.doc.

-Bill

```
/*=====
```

```
Program:   Visualization Toolkit
Module:    $RCSfile: vtkImageHessianResponse.cxx,v $
Language:  C++
Date:      $Date: 2002/12/27 13:54:11 $
Version:   $Revision: 1.26 $
```

```
=====*/
```

```
#include "vtkImageData.h"
#include "vtkImageHessianResponse.h"
#include "vtkMath.h"
#include "vtkObjectFactory.h"
#include "vtkPointData.h"
```

```
#define IXX VTK_HESSIANRESPONSE_IXX
#define IXY VTK_HESSIANRESPONSE_IXY
#define IXZ VTK_HESSIANRESPONSE_IXZ
#define IYX VTK_HESSIANRESPONSE_IYX
#define IYY VTK_HESSIANRESPONSE_IYY
#define IYZ VTK_HESSIANRESPONSE_IYZ
#define IZX VTK_HESSIANRESPONSE_IZX
#define IZY VTK_HESSIANRESPONSE_IZY
#define IZZ VTK_HESSIANRESPONSE_IZZ
#define I   VTK_HESSIANRESPONSE_I
```

```
//-----
vtkImageHessianResponse* vtkImageHessianResponse::New()
{
    // First try to create the object from the vtkObjectFactory
    vtkObject* ret = vtkObjectFactory::CreateInstance("vtkImageHessianResponse");
    if(ret)
    {
        return (vtkImageHessianResponse*)ret;
    }
    // If the factory was unable to create the object, then create it here.
    return new vtkImageHessianResponse;
}
```

```
//-----
```

```
// Constructor sets default values
vtkImageHessianResponse::vtkImageHessianResponse()
{
    this->Gamma12 = 1.0;
    this->Gamma23 = 1.0;
    this->Alpha = 0.25;
    this->LowerIntensityThresh = -VTK_LARGE_FLOAT;
    this->UpperIntensityThresh = VTK_LARGE_FLOAT;
    this->SetResponseTypeToSheet();
    this->VectorData = vtkFloatArray::New();
    this->VectorData->SetNumberOfComponents(3);
    this->ScalarData = vtkFloatArray::New();
    this->ScalarData->SetNumberOfComponents(1);
    this->SelectedEigenvector = 0;
}
```

```

//-----
// Destructor cleans up
vtkImageHessianResponse::~vtkImageHessianResponse()
{
    cout << "vtkImageHessianResponse::~vtkImageHessianResponse. now entering" <<
endl;
    this->VectorData->Delete();
    this->ScalarData->Delete();
}

//-----
void vtkImageHessianResponse::ExecuteInformation ( vtkImageData **inData,
                                                    vtkImageData *outData )
{
    outData->SetScalarType(VTK_FLOAT);
}

//-----
typedef float (*ResponseFunctionPtr) ( vtkImageHessianResponse* self, float
*eigenvalue, float **eigenvector );

//-----
static float vtkImageHessianSheetFunction ( vtkImageHessianResponse* self, float
*eigenvalue, float **eigenvector )
{
    float maxL, midL, minL;
    float response;

    // Parameters
    float Gamma12 = self->GetGamma12();
    float Gamma23 = self->GetGamma23();
    float Alpha = self->GetAlpha();

    // eigenvalues are already sorted by magnitude
    maxL = fabs (eigenvalue[0]);
    midL = fabs (eigenvalue[1]);
    minL = fabs (eigenvalue[2]);

    // no longer works because signed sorting has been removed
    if (0) {
        //only look at places where the eigenvalues are all negative
        if (maxL >= 0) return 0;

        //float fact0 = exp(-maxL);
        float fact1 = fabs(log(1-minL));
        float fact2 = fabs(log(midL/minL));
        //float fact3 = pow((1+midL/minL),0.5);
        //float fact4 = log(-midL);
        //float fact5 = log(midL/maxL);

        if (fact1*fact2 < 1) return 0;

        response = fabs(log(fact1*fact2));
    }
}

```

```

    response = maxL - (Gamma12*midL + minL);
    if (response < 0.0) {
        response = 0.0;
    }

    return response;
}

//-----
static float vtkImageHessianLineFunction ( vtkImageHessianResponse* self, float
*eigenvalue, float **eigenvector )
{
    float l1, l2, l3;
    // Parameters
    float Gamma12 = self->GetGamma12();
    float Gamma23 = self->GetGamma23();
    float Alpha = self->GetAlpha();
    l1 = eigenvalue[0]; l2 = eigenvalue[1]; l3 = eigenvalue[2];

    float l123 = 0.0;
    if ( l1 <= 0.0 && l2 < 0.0 && l3 < 0.0 )
    {
        l123 = fabs ( l3 ) *
            pow ( static_cast<float>(l2 / l3), Gamma23 ) *
            pow ( static_cast<float>(1.0 + l1 / fabs ( l2 )), Gamma12 );
    }
    else
    {
        if ( ( fabs ( l2 ) / Alpha ) > l1 && l1 > 0.0 && l2 < 0.0 && l3 < 0.0 )
        {
            l123 = fabs ( l3 ) *
                pow ( static_cast<float>(l2 / l3), Gamma23 ) *
                pow ( static_cast<float>(1.0 + l1 / fabs ( l2 )), Gamma12 );
        }
        else
        {
            l123 = 0.0;
        }
    }
    return l123;
}

//-----
static float vtkImageHessianSphereFunction ( vtkImageHessianResponse* self,
float *eigenvalue, float **eigenvector )
{
    // Want to measure how "equal" the eigen values are. They should
    // all be negative and roughly equal. The response should be the
    // smallest in absolute value weighted by a function that decreases
    // with the difference between them.
    float l1, l2, l3;
    l1 = eigenvalue[0]; l2 = eigenvalue[1]; l3 = eigenvalue[2];

    if ( l1 > 0.0 )
    {
        return 0.0;
    }
}

```

```

// Set the weight as a ratio of ( l3 - l1 ) / l2.
// will be maximum when l1 ~ l2 ~ l3

float w;
w = ( l3 - l1 ) / l2;
return -l3 * pow (static_cast<float>(w), self->GetGamma12() );
}

//-----
// Copies eigenvalues from eigenvalue to outvalue, but
// just changes pointer for outvector
// avoids expensive copy for each element of eigenvector
void SortVectorsByMagnitude(float* eigenvalue, float** eigenvector,
                           float* outvalue, float** outvector)
{
    float abs11 = fabs ( eigenvalue[0] );
    float abs12 = fabs ( eigenvalue[1] );
    float abs13 = fabs ( eigenvalue[2] );

    if ( abs11 >= abs12 ) {
        if ( abs11 >= abs13 ) {
            outvalue[0] = eigenvalue[0];
            outvector[0] = eigenvector[0];
            if ( abs12 >= abs13 ) {
                outvalue[1] = eigenvalue[1];
                outvector[1] = eigenvector[1];
                outvalue[2] = eigenvalue[2];
                outvector[2] = eigenvector[2];
            }
            else {
                outvalue[1] = eigenvalue[2];
                outvector[1] = eigenvector[2];
                outvalue[2] = eigenvalue[1];
                outvector[2] = eigenvector[1];
            }
        }
        else {
            // L1 > L2, L3 > L1
            outvalue[0] = eigenvalue[2];
            outvector[0] = eigenvector[2];
            outvalue[1] = eigenvalue[0];
            outvector[1] = eigenvector[0];
            outvalue[2] = eigenvalue[1];
            outvector[2] = eigenvector[1];
        }
    }
    else {
        // L2 > L1
        if ( abs12 >= abs13 ) {
            // L2 > L3
            outvalue[0] = eigenvalue[1];
            outvector[0] = eigenvector[1];
            if ( abs11 >= abs13 ) {
                // L1 > L3
                outvalue[1] = eigenvalue[0];
            }
        }
    }
}

```

```

        outvector[1] = eigenvector[0];
        outvalue[2] = eigenvalue[2];
        outvector[2] = eigenvector[2];
    }
    else {
        outvalue[1] = eigenvalue[2];
        outvector[1] = eigenvector[2];
        outvalue[2] = eigenvalue[0];
        outvector[2] = eigenvector[0];
    }
}
else {
    // L3 > L2, L2 > L1
    outvalue[0] = eigenvalue[2];
    outvector[0] = eigenvector[2];
    outvalue[1] = eigenvalue[1];
    outvector[1] = eigenvector[1];
    outvalue[2] = eigenvalue[0];
    outvector[2] = eigenvector[0];
}
}
}

```

//-----

// This templated function executes the filter for any type of data.

template <class T>

```

static void vtkImageHessianResponseExecute ( vtkImageHessianResponse *self,
                                             vtkImageData *outData,
                                             int outExt[6], int id,
                                             T* vtkNotUsed ( dummy ) )

```

```

{
    int i, j;
    unsigned long count = 0;
    unsigned long target;
    int myeigenvec;
    int numC;
    int inIncX, inIncY, inIncZ;
    int outIncX, outIncY, outIncZ;
    int maxX, maxY, maxZ;
    int idxC, idxX, idxY, idxZ;
    float l123;
    ResponseFunctionPtr RFP;

    switch ( self->GetResponseType() )
    {
        case VTK_HESSIAN_RESPONSE_SHEET:
            RFP = vtkImageHessianSheetFunction;
            break;
        case VTK_HESSIAN_RESPONSE_SPHERE:
            RFP = vtkImageHessianSphereFunction;
            break;
        case VTK_HESSIAN_RESPONSE_LINE:
        default:
            RFP = vtkImageHessianLineFunction;
            break;
    }
}

```

```

T* Hessian[7];
vtkDataObject **InputsDO = self->GetInputs();
vtkImageData* Inputs[7];
float* outPtr;

myeigenvec = self->GetSelectedEigenvector();

// Eigen vectors and values
float *raw_eigenvalue = new float[3];
float **raw_eigenvector = new float*[3];
float *eigenvalue = new float[3];
float **eigenvector = new float*[3];
float **qmatrix = new float*[3];
for (i = 0; i < 3; i++) {
    qmatrix[i] = new float[3];
    raw_eigenvector[i] = new float[3];
    raw_eigenvalue[i] = 0.0;
    eigenvector[i] = raw_eigenvector[i];
    eigenvalue[i] = 0.0;
    for (j = 0; j < 3; j++) {
        raw_eigenvector[i][j] = 0.0;
    }
}

for ( i = 0; i < 7; ++i )
{
    Inputs[i] = (vtkImageData*)InputsDO[i];
}

numC = Inputs[0]->GetNumberOfScalarComponents();
// find the region to loop over
maxX = outExt[1] - outExt[0];
maxY = outExt[3] - outExt[2];
maxZ = outExt[5] - outExt[4];
target = (unsigned long) ((maxZ+1)*(maxY+1)/50.0);
target++;

// Get increments to march through data
Inputs[0]->GetContinuousIncrements(outExt, inIncX, inIncY, inIncZ);
outData->GetContinuousIncrements(outExt, outIncX, outIncY, outIncZ);

outPtr = (float*) outData->GetScalarPointerForExtent ( outExt );

// Fill in the Hessian pointers
Hessian[IXY] = (T*) Inputs[IXY]->GetScalarPointerForExtent ( outExt );
Hessian[IXZ] = (T*) Inputs[IXZ]->GetScalarPointerForExtent ( outExt );
Hessian[IYZ] = (T*) Inputs[IYZ]->GetScalarPointerForExtent ( outExt );

Hessian[IXX] = (T*) Inputs[IXX]->GetScalarPointerForExtent ( outExt );
Hessian[IYY] = (T*) Inputs[IYY]->GetScalarPointerForExtent ( outExt );
Hessian[IZZ] = (T*) Inputs[IZZ]->GetScalarPointerForExtent ( outExt );

Hessian[I] = (T*) Inputs[I]->GetScalarPointerForExtent ( outExt );

T lowThresh, upperThresh;

// Make sure the replacement values are within the output scalar range

```

```

if (self->GetLowerIntensityThresh() < (float) Inputs[0]->GetScalarTypeMin())
{
    lowThresh = (T) Inputs[0]->GetScalarTypeMin();
}
else
{
    lowThresh = (T) self->GetLowerIntensityThresh();
}

if (self->GetUpperIntensityThresh() > (float) Inputs[0]->GetScalarTypeMax())
{
    upperThresh = (T) Inputs[0]->GetScalarTypeMax();
}
else
{
    upperThresh = (T) self->GetUpperIntensityThresh();
}

// Loop through ouput pixels
for (idxZ = 0; idxZ <= maxZ; idxZ++)
{
    for (idxY = 0; !self->AbortExecute && idxY <= maxY; idxY++)
    {
        if (!id)
        {
            if (!(count%target))
            {
                self->UpdateProgress(count/(50.0*target));
            }
            count++;
        }
        for (idxX = 0; idxX <= maxX; idxX++)
        {
            for ( idxC = 0; idxC < numC; idxC++ )
            {
                if ((*Hessian[I])) >= lowThresh && ((*Hessian[I])) <= upperThresh)
                {
                    // Fill in the Hessian
                    qmatrix[0][0] = (float) ((*Hessian[IXX]));
                    qmatrix[0][1] = (float) ((*Hessian[IXY]));
                    qmatrix[0][2] = (float) ((*Hessian[IXZ]));

                    qmatrix[1][0] = (float) ((*Hessian[IYX]));
                    qmatrix[1][1] = (float) ((*Hessian[IYY]));
                    qmatrix[1][2] = (float) ((*Hessian[IYZ]));

                    qmatrix[2][0] = (float) ((*Hessian[IZX]));
                    qmatrix[2][1] = (float) ((*Hessian[IZY]));
                    qmatrix[2][2] = (float) ((*Hessian[IZZ]));

                    int status =
vtkMath::Jacobi(qmatrix,raw_eigenvalue,raw_eigenvector );
                    if ( !status ) {
                        vtkGenericWarningMacro ( << "vtkImageHessianResponse: Jacobi
returned error" );
                        l123 = 0.0;

```



```

        }
        else
        {
SortVectorsByMagnitude(raw_eigenvalue,raw_eigenvector,eigenvalue,eigenvector);
        l123 = (*RFP) (self,eigenvalue,eigenvector);
        }
    }
    else
    {
        l123 = 0.0;
    }

    *outPtr = l123;
    self->GetScalarData()->InsertNextTuple1(eigenvalue[myeigenvec]);
    self->GetVectorData()->InsertNextTuple3(eigenvector[myeigenvec][0],
                                            eigenvector[myeigenvec][1],
                                            eigenvector[myeigenvec][2]);

    for ( i = 0; i < 7; i++ )
    {
        ++Hessian[i];
    }
    ++outPtr;
}
for ( i = 0; i < 7; i++ )
{
    Hessian[i] += inIncX;
}
outPtr += outIncX;
}
outPtr += outIncY;
for ( i = 0; i < 7; i++ )
{
    Hessian[i] += inIncY;
}
}
outPtr += outIncZ;
for ( i = 0; i < 7; i++ )
{
    Hessian[i] += inIncZ;
}
}

for (i = 0; i < 3; i++)
{
    delete[] qmatrix[i];
    delete[] raw_eigenvector[i];
}
delete[] qmatrix;
delete[] raw_eigenvector;
delete[] raw_eigenvalue;
delete[] eigenvector;
delete[] eigenvalue;

// assign the vectors to the image data
outData->GetPointData()->SetVectors(self->GetVectorData());
//outData->GetPointData()->SetScalars(self->GetScalarData());

```

```

self->GetScalarData()->SetName("eigenvalues");
outData->GetPointData()->AddArray(self->GetScalarData());

}

//-----
// This method is passed a input and output data, and executes the filter
// algorithm to fill the output from the input.
// It just executes a switch statement to call the correct function for
// the data's data types.
void vtkImageHessianResponse::ThreadedExecute(vtkImageData **inData,
                                              vtkImageData *outData,
                                              int outExt[6], int id)
{
    int i, j;
    bool valid;
    int *outExtent;
    int dataType;
    if ( GetNumberOfInputs() != 7 )
    {
        vtkErrorMacro ( << "Execute: vtkImageHessianResponse requires 7 inputs" );
        return;
    }

    vtkDataObject **Inputs = GetInputs();
    outExtent = Inputs[0]->GetWholeExtent();
    dataType = ((vtkImageData*)Inputs[0])->GetScalarType();
    valid = 1;
    for ( i = 0; i < 7; ++i )
    {
        vtkImageData* in;
        in = (vtkImageData*) Inputs[i];

        // Do all of our checks
        valid = valid && ( dataType == in->GetScalarType() );
        if ( !valid )
        {
            vtkErrorMacro ( << "Execute: vtkImageHessianResponse datatype mis-match on
input" );
            return;
        }
        int *ext = in->GetWholeExtent();
        for ( j = 0; j < 6; ++j )
        {
            valid = valid && ( ext[j] == outExtent[j] );
        }
        valid = valid && in->GetNumberOfScalarComponents() ==
((vtkImageData*)Inputs[0])->GetNumberOfScalarComponents();
        if ( !valid )
        {
            vtkErrorMacro ( << "Execute: vtkImageHessianResponse extent mis-match on
input" );
            return;
        }
    }
}

```

```

switch (inData[0]->GetScalarType())
{
    vtkTemplateMacro5(vtkImageHessianResponseExecute, this,
                      outData, outExt, id, static_cast<VTK_TT*>(0));
    default:
        vtkErrorMacro(<< "Execute: Unknown ScalarType");
        return;
}
)

void vtkImageHessianResponse::PrintSelf(ostream& os, vtkIndent indent)
{
    vtkImageMultipleInputFilter::PrintSelf(os, indent);

    os << indent << "Gamma12: " << this->Gamma12 << "\n";
    os << indent << "Gamma23: " << this->Gamma23 << "\n";
    os << indent << "Alpha: " << this->Alpha << "\n";
    if (this->ResponseType == VTK_HESSIAN_RESPONSE_LINE)
    {
        os << indent << "ResponseType: LINE" << "\n";
    }
    else if (this->ResponseType == VTK_HESSIAN_RESPONSE_SPHERE)
    {
        os << indent << "ResponseType: SPHERE" << "\n";
    }
    else
    {
        os << indent << "ResponseType: UNKNOWN" << "\n";
    }
}

```

**This Page is Inserted by IFW Indexing and Scanning
Operations and is not part of the Official Record**

BEST AVAILABLE IMAGES

Defective images within this document are accurate representations of the original documents submitted by the applicant.

Defects in the images include but are not limited to the items checked:

- ☐ BLACK BORDERS
- ☐ IMAGE CUT OFF AT TOP, BOTTOM OR SIDES
- ☐ FADED TEXT OR DRAWING
- ☐ BLURRED OR ILLEGIBLE TEXT OR DRAWING
- ☐ SKEWED/SLANTED IMAGES
- ☐ COLOR OR BLACK AND WHITE PHOTOGRAPHS
- ☒ GRAY SCALE DOCUMENTS
- ☒ LINES OR MARKS ON ORIGINAL DOCUMENT
- ☐ REFERENCE(S) OR EXHIBIT(S) SUBMITTED ARE POOR QUALITY
- ☐ OTHER: _____

IMAGES ARE BEST AVAILABLE COPY.

As rescanning these documents will not correct the image problems checked, please do not report these problems to the IFW Image Problem Mailbox.